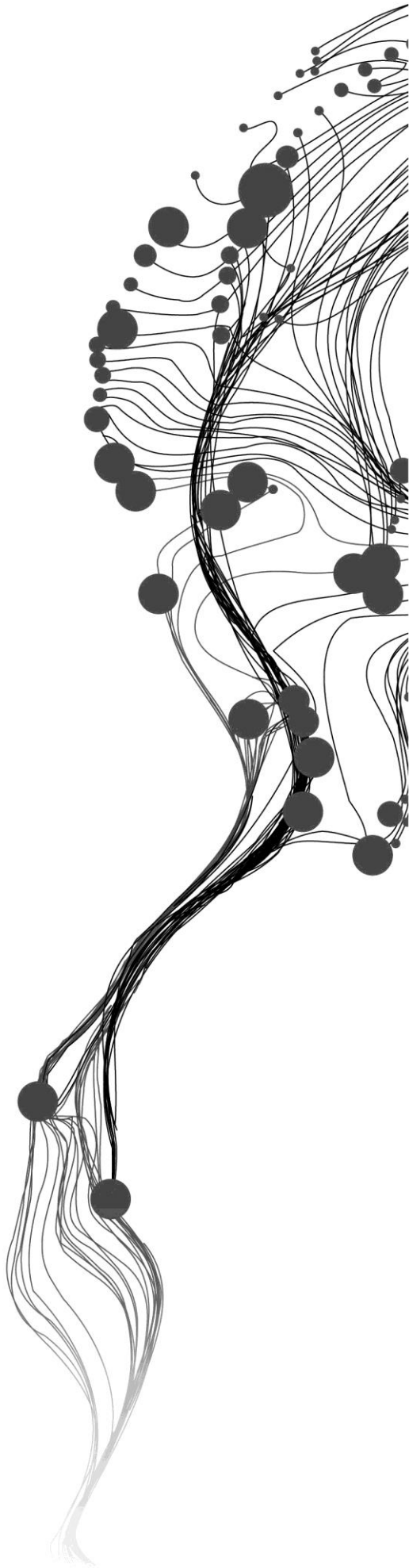


# **Mapping of biophysical and biochemical properties of coastal tidal wetland habitats with Landsat 8**

ZHU NANHUANUOWA  
February, 2017

SUPERVISORS:  
Dr.ir. C. van der Tol  
Dr.ir. C.M.M. Mannaerts



# Mapping of biophysical and biochemical properties of coastal tidal wetland habitats with Landsat 8

ZHU NANHUANUOWA

Enschede, The Netherlands, [02, 2017]

Thesis submitted to the Faculty of Geo-Information Science and Earth Observation of the University of Twente in partial fulfilment of the requirements for the degree of Master of Science in Geo-information Science and Earth Observation.

Specialization: [Water resource]

## SUPERVISORS:

Dr.ir. C. van der Tol

Dr.ir. C.M.M. Mannaerts

## THESIS ASSESSMENT BOARD:

[Dr. Ir. S. Salama (Chair)]

[Dr. Shi Chen (External Examiner, CNU)]

#### DISCLAIMER

This document describes work undertaken as part of a programme of study at the Faculty of Geo-Information Science and Earth Observation of the University of Twente. All views and opinions expressed therein remain the sole responsibility of the author, and do not necessarily represent those of the Faculty.

## ABSTRACT

The objectives of this research were to map of LAI, chlorophyll content as well as the sensible heat flux, latent heat flux and productivity in Chongming Dongtan coastal tidal wetland habitats of China and to provide a mapping protocol of biophysical and biochemical properties in Chongming Dongtan wetland for environmental protection and restoration as well as assessment and monitoring.

In order to obtain significant information for biodiversity protection and management, a method based on the SCOPE model and Lookup Table approach has been developed. Firstly, the SCOPE model was calibrated to match in situ reflectance spectra with simulated reflectance spectra from model through adjusting parameter values and obtain the simulated LAI, Cab, GPP, sensible heat flux, latent heat flux and reflectance spectra for sample points. Then the Landsat 8 OLI bands reflectance was compared with SCOPE simulated reflectance, to find a best fit of reflectance for the respective pixel (Lookup Table approach), resulting in corresponding LAI, Cab, sensible heat flux, GPP and latent heat flux to map of biophysical and biochemical properties.

The results derived from this study contain the peak value of *Spartina alterniflora* reflectance spectrum is the highest (0.43), whereas *Phragmites australis* (0.17) is the second and *Scirpus mariqueter* (0.14) is the third. The peak value of mudflats reflectance spectrum is the lowest one (0.13). Meanwhile, the reflectance values of *Scirpus mariqueter* and *Phragmites australis* spectra are lower than those commonly found for vegetated areas. This may be caused by the dark soil background and low leaf area index. Meanwhile, the causes of the differences between Landsat 8 TOC reflectance and in situ reflectance in the same pixel are: (1) meteorological influence; (2) spatial resolution; (3) the quantity of field work data.

Moreover, as for the values of latent heat flux and productivity, mudflats are lower than vegetation. However, the values of sensible heat flux of mudflats are higher than that of vegetation. Furthermore, the uncertainties of the productivity product of the SCOPE model from Landsat 8 are: (1) uncertain meteorological condition; (2) insufficient simulation of mudflats; (3) the quality and quantity of field work data; (4) the number of simulated combinations.

## ACKNOWLEDGEMENTS

I really appreciate the International Institute for Geo-Information Science and Earth Observation (ITC) and Capital Normal University (CNU) for providing me with the precious opportunity to study in Netherlands. I have learned a lot from some professors and broadened the horizon.

My special thanks are addressed to my supervisors, Dr.ir. C. van der Tol and Dr.ir. C.M.M. Mannaerts, for their patient guidance and kind support. It is my honor that I can finish my MSc topic under your attention.

My genuine thanks go to Dr.ir. S. Salama and ir. A.M. van Lieshout. Thanks for your lots of useful suggestions and fantastic ideas at the proposal and midterm period.

I also want to thank my friends for accompanying with me a lot and helping me in my living and studying.

Finally, my deepest thanks go to my father and my mother. Thank you for your support and encouragement. Without your love and help, I could not have completed this research.

# TABLE OF CONTENTS

---

|   |     |
|---|-----|
| List of figures.....  | v   |
| List of tables .....  | vii |
| <br>  |     |
| 1. INTRODUCTION .....   | 1   |
| 1.1. Background.....  | 1   |
| 1.2. Problem Definition.....  | 3   |
| 1.3. Research Objectives.....   | 3   |
| 1.3.1. Overall Objectives .....   | 3   |
| 1.3.2. Specific Objectives.....   | 3   |
| 1.4. Research Questions.....  | 4   |
| 1.5. Structure of the Thesis.....   | 4   |
| 2. MATERIALS & METHODOLOGY .....  | 7   |
| 2.1. Study Area.....  | 7   |
| 2.1.1. Location & Climate.....  | 7   |
| 2.1.2. Vegetation Types.....  | 8   |
| 2.2. Study Materials.....   | 9   |
| 2.2.1. Landsat 8 Image & Landsat 5 Image .....  | 9   |
| 2.2.2. Meteorological Data .....  | 10  |
| 2.2.3. Flux Tower Data .....  | 11  |
| 2.2.4. Field Data Support.....  | 11  |
| 2.2.5. Software & Techniques Support .....  | 14  |
| 2.3. Research Methodology .....   | 15  |
| 2.3.1. Data Pre-processing of Landsat Image .....   | 16  |
| 2.3.2. Model Calibration with In Situ Data.....   | 16  |
| 2.3.3. Simulated Maps from SCOPE Model with Landsat 8 Data .....  | 17  |
| 2.3.4. Model Validation.....  | 19  |
| 3. RESULTS.....   | 21  |
| 3.1. Results of Atmospheric Correction for Landsat images using ILWIS SMAC Toolbox.....                               | 21  |
| 3.1.1. Input Data of SMAC Toolbox in ILWIS.....   | 21  |
| 3.1.2. Results of TOC Reflectance after AC Process.....   | 23  |
| 3.2. Results & Analysis of Model Calibration with Measurements and Simulations .....                                  | 24  |
| 3.2.1. Mudflats .....   | 24  |
| 3.2.2. Vegetation .....   | 26  |
| 3.3. Mapping of Productivity, Latent Heat Flux, Sensible Heat Flux and Vegetation parameters (LAI & Chlorophyll)..... | 28  |
| 3.3.1. Input Data Selection of SCOPE Model Simulation .....   | 28  |

|  |    |
|--|----|
| 3.3.2. Results of Simulated Reflectance from SCOPE Model .....   | 29 |
| 3.3.3. Maps & Analysis of Productivity, Latent Heat Flux, Sensible Heat Flux and Vegetation<br>parameters (LAI & Chlorophyll)..... | 31 |
| 3.4. Results of Model Validation with Simulations and Measurements.....  | 35 |
| 3.4.1. Results of Simulations with Landsat 5 TM images.....  | 35 |
| 3.4.2. Comparison of Simulation and Flux Tower Data .....  | 35 |
| 4. DISCUSSION.....   | 39 |
| 4.1. Analysis of Selecting Variable Value Range of Input Parameters in SCOPE Model Simulation.....                                 | 39 |
| 4.2. Explanation of Abnormal Reflectance Spectrums in SCOPE Model Simulation .....   | 41 |
| 4.3. Reasons for the Uncertainties of Mapping with SCOPE Model.....  | 41 |
| 5. CONCLUSION.....   | 45 |
| List of references .....   | 47 |

# LIST OF FIGURES

---

|  |    |
|--|----|
| Figure 1 The location of Chongming Dongtan Nature Reserve in Shanghai and a Landsat TM image of July 19, 2004.<br>Profiles I–IV are four elevation transects measured at September 4–11, 2005. (Zheng et al., 2016)..... | 7  |
| Figure 2 Vegetation classification in Chongming Dongtan Nature Reserve (Zheng et al., 2016).....   | 8  |
| Figure 3 The examples of the three main vegetation types in the study area .....   | 9  |
| Figure 4 Measurement metadata information.....   | 11 |
| Figure 5 Landsat 8 image of Chongming Dongtan wetlands on 22nd September, 2016 (band4, 3, 2) and sampling<br>locations and dates .....   | 12 |
| Figure 6 Raw reflectance spectrum of vegetation (left) & spectrum after statistics (right).....  | 13 |
| Figure 7 Raw reflectance spectrum of mudflats (left) & spectrum after statistics (right).....  | 13 |
| Figure 8 Representative Spectrum of <i>Spartina alterniflora</i> , <i>Scirpus mariqueter</i> , <i>Phragmites australis</i> and mudflats ....   | 14 |
| Figure 9 ASD FieldSpec handheld 2 .....  | 14 |
| Figure 10 Flowchart of overall methodology in this research.....   | 15 |
| Figure 11 Flowchart of model calibration process in this research.....   | 17 |
| Figure 12 Flowchart of the Lookup Table approach in this research.....   | 18 |
| Figure 13 Flowchart of model validation process in this research.....  | 20 |
| Figure 14 AOT of Taihu station on 3 <sup>rd</sup> September in 2016.....   | 21 |
| Figure 15 Water vapor of Taihu station on 3 <sup>rd</sup> September in 2016 .....  | 22 |
| Figure 16 Total ozone map on 22 <sup>nd</sup> September in 2016 .....  | 22 |
| Figure 17 TOC reflectance after AC of Landsat 8 image in Dongtan on September 22 <sup>nd</sup> , 2016 (band4, 3, 2).....   | 23 |
| Figure 18 (a) The ocean reflectance spectrum (M.J.A. Butler et al., 1988); (b) The reflectance spectra of one pixel of<br>the first 7 bands of Landsat 8 in the ocean part after atmospheric correction.....             | 24 |
| Figure 19 The simulated (gray line) and measuring (blue line) reflectance spectrums of mudflats in each sample point<br>.....  | 25 |
| Figure 20 The total simulated and measuring reflectance spectrums of mudflats.....   | 25 |
| Figure 21 The RMSE value between simulations & measurements of mudflats in each sample point .....   | 26 |
| Figure 22 The total curves and RMSE value between simulations & measurements of three vegetation types: (a)<br><i>Phragmites australis</i> ; (b) <i>Scirpus mariqueter</i> ; (c) <i>Spartina alterniflora</i> .....      | 27 |
| Figure 23 The simulated reflectance spectrums corresponding to Landsat 8 OLI band sensitivity.....   | 30 |
| Figure 24 Landsat 8 OLI band sensitivity.....  | 30 |
| Figure 25 Spectra of SCOPE simulated reflectance's extracted only in Landsat 8 first seven bands.....  | 31 |
| Figure 26 Map of RMSE between models simulated reflectance and Landsat 8 OLI pixel reflectance in Chongming<br>Dongtan.....  | 32 |
| Figure 27 Map of leaf chlorophyll content ( $\mu\text{g cm}^{-2}$ ) in Chongming Dongtan.....  | 32 |
| Figure 28 Map of LAI ( $\text{m}^2 \text{m}^{-2}$ ) in Chongming Dongtan.....  | 33 |
| Figure 29 Map of productivity ( $\mu\text{molm}^{-2}\text{s}^{-1}$ ) in Chongming Dongtan.....   | 33 |
| Figure 30 Map of latent heat flux ( $\text{W m}^{-2}$ ) in Chongming Dongtan.....  | 34 |
| Figure 31 Map of sensible heat flux ( $\text{W m}^{-2}$ ) in Chongming Dongtan.....  | 34 |
| Figure 32 The simulated and measured curves of latent heat flux in the year of 2005:.....  | 37 |

|  |    |
|--|----|
| Figure 33 The simulated and measured curves of sensible heat flux in the year of 2005:.....  | 38 |
| Figure 34 The simulated maps of productivity, latent heat flux, sensible heat flux, LAI, chlorophyll and RMSE with combination of 46 measuring points .....              | 39 |
| Figure 35 The simulated maps of productivity, latent heat flux, sensible heat flux, LAI, chlorophyll and RMSE with combination of LAI & chlorophyll without 0 value..... | 40 |
| Figure 36 The simulated reflectance spectrums at the wavelength between 400nm and 900 nm.....  | 41 |
| Figure 37 The simulated maps of productivity, latent heat flux, sensible heat flux, LAI, chlorophyll and RMSE before removing.....                                       | 42 |
| Figure 38 The simulated maps of LAI with two selecting points.....   | 42 |
| Figure 39 The 5 simulated reflectance spectrums and pixel values in 7 bands of Landsat 8 in vegetated area.....  | 43 |
| Figure 40 The 5 simulated reflectance spectrums and pixel values in 7 bands of Landsat 8 in mudflats area.....   | 43 |

## LIST OF TABLES

---

|  |    |
|--|----|
| Table 1 Band combinations of Landsat 8 OLI and TIRS image .....  | 9  |
| Table 2 Band combinations of Landsat 5 TM image .....  | 10 |
| Table 3 Software and techniques used in this study .....   | 14 |
| Table 4 Necessary parameters and their data source of Atmospheric Correction.....  | 16 |
| Table 5 The final input data of SMAC.....  | 22 |
| Table 6 The maximum, minimum and mean values of 4 soil parameters in RTMo retrievals.....  | 26 |
| Table 7 The maximum, minimum and mean values of 9 vegetation parameters for 3 vegetation types in RTMo retrievals.....                               | 28 |
| Table 8 The meteorological conditions used for the simulation of fluxes in the LUT.....  | 29 |
| Table 9 The values selection of Cab, Cca and LAI in SCOPE model input data.....  | 29 |
| Table 10 The values of LAI and chlorophyll content around the two flux towers from 2005 to 2007 .....  | 35 |
| Table 11 The RMSE values of simulated and measured of latent heat flux (LE) and sensible heat flux (H) in the two flux towers from 2005 to 2007..... | 38 |
| Table 12 The values selection of Cab and LAI in SCOPE model input data.....  | 40 |



# 1. INTRODUCTION

## 1.1. Background

Tidal wetlands are significant and vulnerable aquatic ecosystems. They are present all around the world, and serve as a kind of critical habitat for extensive varieties of fish, plants and other wildlife (Turpie et al., 2015). This sort of ecosystem contributes to protecting and buffering shorelines, adjusting river runoff, controlling and storing floodwaters potentially as well as purifying natural water bodies, etc. (Levin, Elron, & Gasith, 2009). Moreover, as rapid growth of carbon dioxide from the air in recent years, tidal wetlands have become carbon sinks for atmospheric GHG due to the enormous Carbon Sequestration Potential (CSP) (Hu et al., 2016). Nevertheless, these habitats are rapidly declining in area due to destruction by natural and human activities such as other species invasion (Chen et al., 2012), sea-level rise (Bhuiyan & Dutta, 2012) and rapid urbanization (Tian et al., 2010), etc. Therefore, monitoring and protecting tidal wetlands, especially for coastal tidal wetlands, is important and valuable not only for ecosystem biodiversity, but also for human sustainable development.

An effective wetland monitoring method for conservation and management should be integrated in nature, including multifarious significant aspects such as properties, distribution, productivity and components (Tuxen et al., 2011). Nevertheless, conventional monitoring methods, which depend on sampling in field work to research characteristics of wetland, are usually time consuming, expensive, and insufficient for analyzing the extensive regional difference and variability of time and space (de Almeida et al., 2015). Remote sensing techniques using satellite sensors supplies an economical and convenient method to onerous field work for assessing, monitoring and protecting coastal tidal wetland and its dynamic variations in different resolutions and scale levels (Wigand et al., 2011).

Over the past decade, developments in remote sensing techniques and rising availability of high spectral and spatiotemporal resolution data have obviously improved our capacity to map properties of wetland habitats (Gilmore et al., 2008). Multi-resolution spatiotemporal images from satellite such as MODIS, Landsat and ASTER are available for free to the public and such sensors have been used in a few researches for the classification of wetland ecosystems (Sieben, Collins, Mtshali, & Venter, 2016; Tana, Letu, Cheng, & Tateishi, 2013). Furthermore, some relatively high resolution sensors just as Quickbird, SPOT, and RapidEye have been used by several studies for classification of dynamic detection analysis in wetland habitats (Wentao, Bingfang, Hongbo, & Hua, 2014; Hong, Kim, Wdowinski, & Feliciano, 2015).

Remote sensing technique in wetland is more difficult than that of terrestrial vegetation due to the fact that coastal interface of wetland habitats that weakens the near-infrared (NIR) signal intensity, transfers red-edge locations, and eventually reduces effects of red-edge type indices and NDVI to detect

vegetation growing (Guo & Guo, 2016; Siciliano, Wasson, Potts, & Olsen, 2008; Mutanga, Adam, & Cho, 2012). Wetland habitats show relatively high spatial and spectral variations as well because of the sudden changes of conditions in surrounding environments that generate limited ecotone areas, making plant community boundary identification difficult (Prospere, McLaren, & Wilson, 2014). Vegetation diversity in wetland ecosystem generates diverse species combinations with various bio-chemical components and morphological structures, which, in reverse, produces different spectral performances resulting in difficulties in mapping of coastal tidal wetlands (Pengra, Johnston, & Loveland, 2007; Heumann, Hackett, & Monfils, 2015).

In recent years, some researches for monitoring and evaluating wetland habitats using remote sensing methods as well as varieties of image processing technologies have been concentrated on classification of vegetation communities (Chonglin, 2009; Wright & Gallant, 2007), and depicting the scope of these ecosystems (Dronova, Gong, & Wang, 2011; Goudie, 2013). This sort of mapping supplies essential information about the spatial extent in the past and present and the dynamics changes of wetland coverage. Other remote sensing researches concentrate on analyzing and detecting the biophysical characteristics of coastal tidal wetland habitats using satellite sensors with coarse temporal resolution (Mishra et al., 2012; Mishra, Ghosh, & Cho, 2015). Although these researches supply profound scientific information of biophysical properties (such as LAI, chlorophyll content, etc.), they are always impossible to provide deeper understanding about the spatiotemporal dynamic changes of the tidal wetlands in the long term. Recently, a research developed mapping of tidal wetland biophysical properties for productivity dynamic changes analysis in the long term using MODIS through establishing relationship between VIs and biophysical characteristics (Ghosh, Mishra, & Gitelson, 2016). However, this sort of mapping needs a lot of sampling data in different years and the process of field work is time consuming.

Physically based modelling can be used to relate remote sensing signals to ecosystem characteristics. The Soil Canopy Observation of Photosynthesis and Energy fluxes model (SCOPE) which is a representative soil-vegetation-atmosphere transfer approach combined with radiative transfer models for leaf and canopy (van der Tol et al., 2009) has been used for the combined simulation of fluorescence signals, TOC (Top of Canopy) reflectance and thermal radiation with CO<sub>2</sub>, energy and water (Timmermans et al., 2013). The SCOPE model that takes into account leaf biochemistry processes combining of radiative, mass transfers and turbulent models inside the canopy is applied to surface energy balance, photosynthesis processes and reflectance spectra between 400nm and 5000nm (Duffour et al., 2015). In the visible wavelength range, reflectance reduces with increase in both chlorophyll and LAI values. Meanwhile, Latent heat flux, sensible heat flux and GPP are positively related to LAI and Cab, so that LAI and Cab (and other pigments) can be used to simulate fluxes of H, LE and GPP.

Chongming Dongtan Wetland which is a significant young tidal wetland nature reserve in the Yangtze River Estuary is now under enormous pressure of urbanization as well as an invasive grass species, such as *Spartina alterniflora* (Chen et al., 2012). Earlier works on Chongming Dongtan Wetlands have focused on detection of shoreline changes (Li, Zhou, Zhang, & Kuang, 2014), biodiversity conservation,

study of organic carbon accumulation capability in different tidal wetland soils (Zhang et al., 2011), migratory of water birds (Zou et al., 2016) and researches of quantitative relationships between salt marsh vegetation patterns, soil elevation and tidal channels (Zheng, Zhou, Tian, & Ding, 2016).

## **1.2. Problem Definition**

Few researches have studied on types, distributions and biophysical and biochemical properties (such as chlorophyll content, LAI, sensible heat flux, latent heat flux and gross primary productivity, etc.) of vegetation in tidal wetlands available on the study in Chongming Dongtan Wetland Nature Reserve. Meanwhile, so far, no studies have focused on mapping of biophysical and biochemical properties with relatively high-resolution satellite sensor (Landsat 8) in these coastal tidal wetland habitats. In order to avoid previous study weakness and obtain significant information for biodiversity protection and management, a method based on the SCOPE model and Lookup Table approach will be developed to help fill this knowledge gap.

## **1.3. Research Objectives**

### **1.3.1. Overall Objectives**

The main objective of this study is to map of LAI, chlorophyll content as well as the sensible heat flux, latent heat flux and productivity in Chongming Dongtan coastal tidal wetland habitats of China through SCOPE model and Lookup Table approach using Landsat 8 data.

### **1.3.2. Specific Objectives**

- To calibrate the SCOPE model to match in situ reflectance with simulated reflectance.
- To compare Landsat 8 TOC reflectance to the simulations and select the best fit.
- To simulate time series of sensible heat flux and latent heat flux and compare these with measurements of counterparts collected from flux tower data in Chongming Dongtan wetland habitats.
- To obtain and analyze maps of vegetation parameters (LAI and chlorophyll content), sensible heat flux, latent heat flux and productivity of vegetation and mudflats.

- To provide a mapping protocol of biophysical and biochemical properties in Chongming Dongtan wetland for environmental protection and restoration as well as assessment and monitoring.

#### **1.4. Research Questions**

1. What are the differences of in situ measured spectral signatures of the different vegetation types and the mudflats?
2. What are the causes of the differences between Landsat 8 TOC reflectance and in situ reflectance in the same pixel?
3. What are the differences among the vegetation and mudflats in terms of: Chlorophyll, LAI, sensible heat flux, latent heat flux and productivity?
4. What are the reasons for the uncertainties of mapping with SCOPE Model from Landsat 8?

#### **1.5. Structure of the Thesis**

This thesis consists of five chapters which are as follows:

Chapter 1 introduces the state of the art and scientific background in this research. Especially, it further explained the objectives and significance of writing this thesis, research questions and hypothesis.

Chapter 2 illustrates a specific outline of biophysical and biochemical properties of study area, materials and methodology, data preprocessing of Landsat 8 & Landsat 5 images and preparation for final data analysis.

Chapter 3 depicts the specific input data and results of TOC reflectance after atmospheric correction for Landsat images, analysis of model calibration with measurements and simulations, mapping of productivity, latent heat flux, sensible heat flux and vegetation parameters and model validation with measurements and simulations.

Chapter 4 discusses selecting variable value range of input parameters in SCOPE model simulation, the explanations of abnormal reflectance spectrums in SCOPE model simulation and the reasons for the uncertainties of mapping with SCOPE model.

Chapter 5 concludes the answers that are corresponding to the research questions provided in the first chapter.



## 2. MATERIALS & METHODOLOGY

### 2.1. Study Area

#### 2.1.1. Location & Climate

Chongming Dongtan wetland habitat is located in the mouth of the Yangtze River Estuary in northeastern Shanghai, China (121°50' - 122°05' E, 31°25' - 31°38' N) (**Figure 1**) (Zou et al., 2016). It has an area of approximately 326km<sup>2</sup> and it consists of marshland and tidal channels. The Chongming Dongtan Nature Reserve was listed in the Chinese Protected Wetlands in the year of 1992, as well as regarded as internationally significant under the Ramsar Wetlands Convention in 2001 and also national nature preserve in the year of 2005 (Zheng et al., 2016). It has been regarded as a subtropical monsoon climate, with an average annual rainfall and temperature of 1022 mm and 15.3 °C, respectively (Zou et al., 2016).

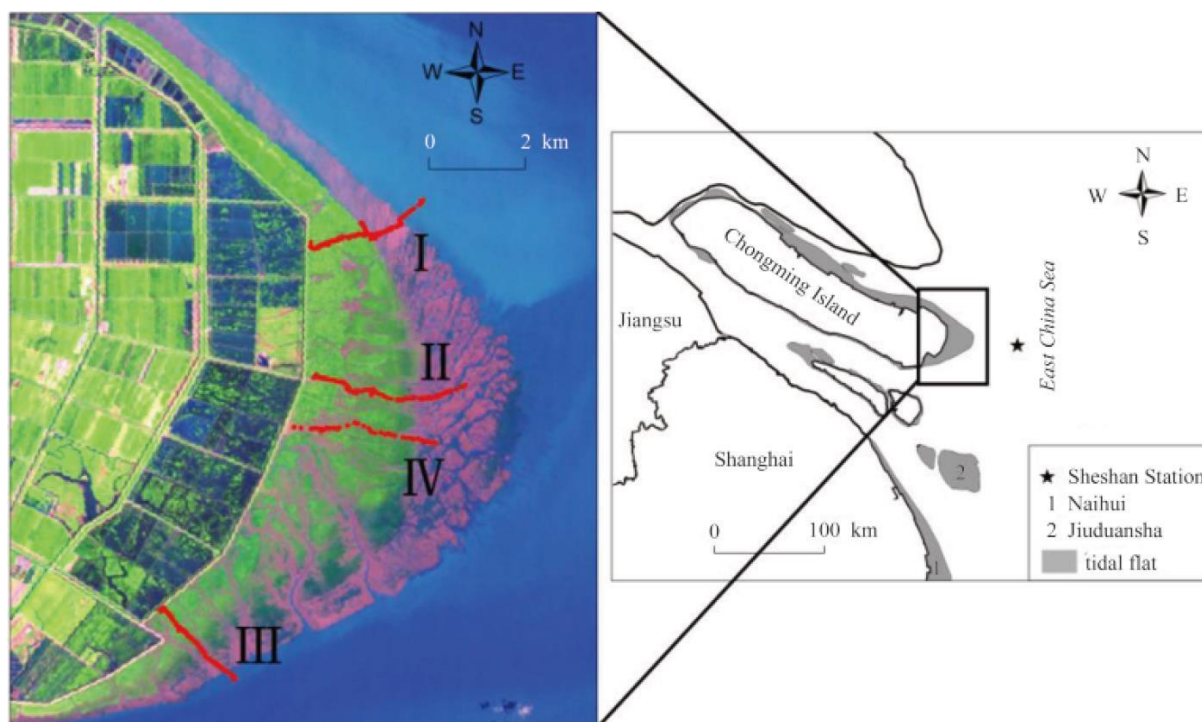


Figure 1 The location of Chongming Dongtan Nature Reserve in Shanghai and a Landsat<sup>TM</sup> image of July 19, 2004. Profiles I–IV are four elevation transects measured at September 4–11, 2005. (Zheng et al., 2016)

### 2.1.2. Vegetation Types

There are several types of vegetation distributed in the study area such as *Scirpus mariqueter*, *Spartina alterniflora*, *Phragmites australis*, oilseed rape, taro, potato and so forth (from field investigation in September, 2016). Meanwhile, the recent literature of which data was collected from the year of 2004 illustrates that there were three dominant vegetation types (*Scirpus mariqueter*, *Spartina alterniflora* and *Phragmites australis*) in Chongming Dongtan wetland habitats (**Figure 2**). *Scirpus mariqueter* community dominates the vegetation at an elevation between 2m and 2.9m in the salt marsh, whereas plant communities are dominated by *Phragmites australis* above 2.9m (Zheng et al., 2016). As for *Spartina alterniflora*, it is a kind of invasive species which could be found on the most elevated soils higher than 3.5m but its spatial distribution is not widespread (Zheng et al., 2016). **Figure 3** describes the examples of the three main vegetation types in Chongming Dongtan wetland habitats.

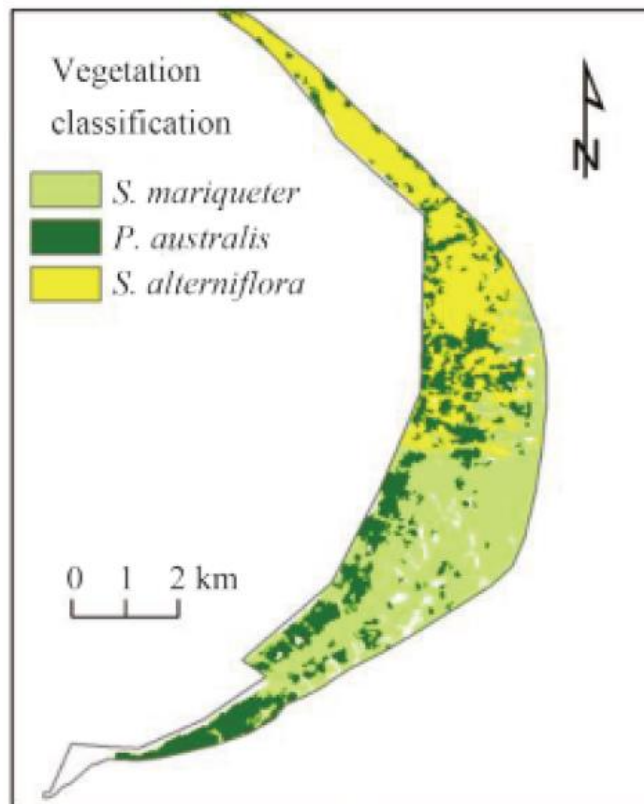


Figure 2 Vegetation classification in Chongming Dongtan Nature Reserve (Zheng et al., 2016)

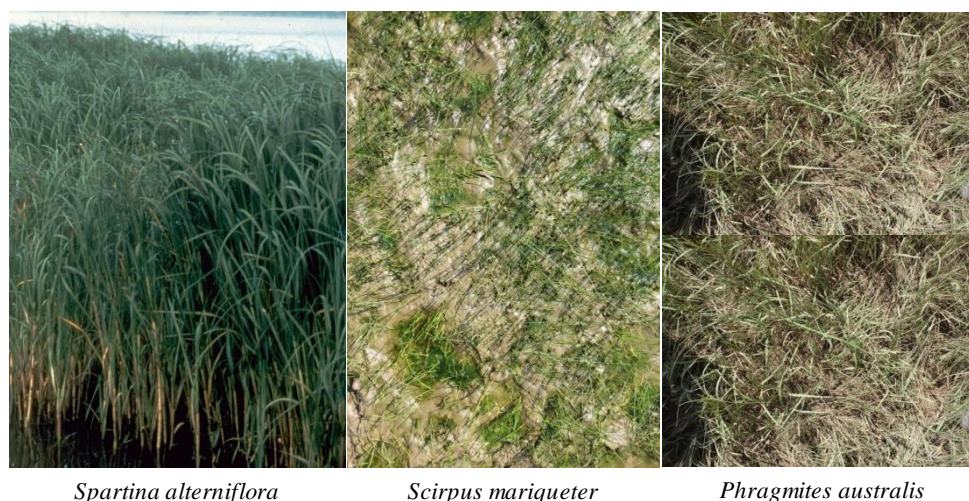


Figure 3 The examples of the three main vegetation types in the study area

## 2.2. Study Materials

### 2.2.1. Landsat 8 Image & Landsat 5 Image

Landsat 8 OLI (Operational Land Imager) and TIRS (Thermal Infrared Sensor) image on 22<sup>nd</sup> September in 2016 was selected for this thesis corresponding to the field data. As **Table 1** shows, the spatial resolution of Landsat 8 image for spectral Bands 1 to 7 and 9 is 30 m. Band 9 of Landsat 8 OLI image is used to detect cirrus cloud. The spatial resolution for Band 8 (panchromatic) is 15 m. Thermal bands 10 and 11 which are collected at 100 m are used to provide fairly more accurate surface temperatures. The spectral range included visible blue (0.45 – 0.51 $\mu\text{m}$ ), visible green (0.53 – 0.59 $\mu\text{m}$ ), visible red (0.64 – 0.67  $\mu\text{m}$ ) and near infrared (0.85 – 0.88  $\mu\text{m}$ ). There were two main reasons for selecting Landsat 8 image for this thesis. On the one hand, Landsat 8 OLI and TIRS images can be obtained freely and its spatial resolution is relatively high compared to MODIS. On the other hand, for validation process, according to flux tower data (year between 2005 and 2007), Landsat 5 images also can be used to complete validation while compared to Sentinel – 2.

Table 1 Band combinations of Landsat 8 OLI and TIRS image

| Landsat 8<br>Operational<br>Land Imager<br>(OLI) and<br>Thermal | Bands                    | Wavelength<br>(micrometers) | Resolution<br>(meters) |
|---|--------------------------|-----------------------------|------------------------|
|   | Band 1 – Coastal aerosol | 0.43 – 0.45                 | 30                     |
|   | Band 2 – Blue            | 0.45 – 0.51                 | 30                     |
|   | Band 3 – Green           | 0.53 – 0.59                 | 30                     |

|   |                                     |               |           |
|---|-------------------------------------|---------------|-----------|
| <b>Infrared<br/>Sensor (TIRS)<br/><br/>Launched<br/>February 11,<br/>2013</b> | Band 4 – Red                        | 0.64 – 0.67   | 30        |
|   | Band 5 – Near Infrared (NIR)        | 0.85 – 0.88   | 30        |
|   | Band 6 – SWIR 1                     | 1.57 – 1.65   | 30        |
|   | Band 7 – SWIR 2                     | 2.11 – 2.29   | 30        |
|   | Band 8 – Panchromatic               | 0.50 – 0.68   | 15        |
|   | Band 9 – Cirrus                     | 1.36 – 1.38   | 30        |
|   | Band 10 – Thermal Infrared (TIRS) 1 | 10.60 – 11.19 | 100* (30) |
|   | Band 11 – Thermal Infrared (TIRS) 2 | 11.50 – 12.51 | 100* (30) |

\*TIRS bands are acquired at 100 meter resolution, but are resampled to 30 meter in delivered data product.

Landsat 5 TM (Thematic Mapper) images in the year between 2005 and 2007 were selected to validate simulated results corresponding to the flux tower data (2005 – 2007). The specific information of Landsat 5 TM (Thematic Mapper) sensor is illustrated in **Table 2**.

**Table 2 Band combinations of Landsat 5 TM image**

| <b>Landsat 5<br/>Thematic<br/>Mapper (TM)</b> | <b>Bands</b>                         | <b>Wavelength<br/>(micrometers)</b> | <b>Resolution<br/>(meters)</b> |
|---|--------------------------------------|-------------------------------------|--------------------------------|
|   | Band 1 –Blue                         | 0.45 – 0.52                         | 30                             |
|   | Band 2 –Green                        | 0.52 – 0.60                         | 30                             |
|   | Band 3 –Red                          | 0.63 – 0.69                         | 30                             |
|   | Band 4 –Near Infrared (NIR)          | 0.76 – 0.90                         | 30                             |
|   | Band 5 – Shortwave Infrared (SWIR) 1 | 1.55 – 1.75                         | 30                             |
|   | Band 6 – Thermal                     | 10.40 – 12.50                       | 120*(30)                       |
|   | Band 7 –Shortwave Infrared (SWIR) 2  | 2.08 – 2.35                         | 30                             |

\* TM Band 6 was acquired at 120-meter resolution, but products are resampled to 30-meter pixels.

## 2.2.2. Meteorological Data

Meteorological data in this research were used to complete atmospheric correction of the Landsat 8 OLI and TIRS image and Landsat 5 TM images. Meteorological data contained aerosol optical thickness, water vapor (g/cm<sup>2</sup>), ozone (g.atm.cm) and surface pressure (hpa). They were collected from Meteorological Station website (<http://data.cma.cn/site/index.html>), Ozone & Air Quality website (<https://ozoneaq.gsfc.nasa.gov/>), and AERONET ([http://aeronet.gsfc.nasa.gov/new\\_web/index.html](http://aeronet.gsfc.nasa.gov/new_web/index.html)).

2.2.3. Flux Tower Data

The flux tower data in this thesis from the year 2005 to 2007 is all from two flux towers: Dongtan 2 Chongming China (31.5847° N, 121.9035° E) and Dongtan 3 Chongming China (31.5169° N, 121.9717° E). The flux tower data was all provided by SKLEC and can supply listing of the variables (air temperature, wind speed, NEE, wind direction, CO<sub>2</sub> flux or the rate of vertical transfer of CO<sub>2</sub>, sensible heat flux, Latent heat flux, etc.), and they provide time series of sensible heat flux and latent heat flux. I did not have GPP processed (only NEE), and therefore limited to H and LE in this study.

2.2.4. Field Data Support

Unfortunately, due to the unfavorable weather conditions and field work time, the author could not take samples in Chongming Dongtan this year. Therefore, data that the author use was made of field data collected earlier by researchers of SKLEC. The data used in the analyses have been collected by Shu Minyan, a Chinese MSc student, who shared measured spectral data in September, 2016.

➤ Measurement metadata

Metadata of the recorded data from the field are shown in **Figure 4**. It provides the information of locations, spectrum number, land cover types, vegetation height, vegetation fraction, soil moisture, weather condition and so forth. Total of 78 samples were obtained, and at least 46 samples of which could be used in this study. They were measured on 9<sup>th</sup>, 10<sup>th</sup>, 12<sup>th</sup>, 13<sup>th</sup>, 20<sup>th</sup>, 21<sup>st</sup>, 22<sup>nd</sup> September, 2016.

|    | A                   | B        | C            | D                                  | E               | F   | G                 | H               | I                     | J            | K             | L              |
|----|---------------------|----------|--------------|------------------------------------|-----------------|---|-------------------|-----------------|-----------------------|--------------|---------------|----------------|
| 1  | 20160909 & 20160910 |          |              |                                    |                 |   |                   |                 |                       |              |               |                |
| 2  | Point               | Latitude | Longitude    | Spectra Number                     | Text Name       | Vegetation Type                                   | Vegetation Height | (Soil Moisture) | (Vegetation Fraction) | (Wind Speed) | (Temperature) | (Air Humidity) |
| 3  | 1                   | 31.46149 | 121.94154    | leaf00000-00009                    |                 | scirpus ariquetar                                 | 8                 | 36.4            | 10                    | 1.8          |               | 27.3           |
| 4  | 2                   |          | 10-19        |                                    |                 | 2.01E+09 scirpus ariquetar                        | 10                | 33.4            | 55                    |              |               |                |
| 5  | 3                   |          | 20-29        |                                    |                 | 2.01E+09 scirpus ariquetar                        | 16.5              | 45.1            |                       |              |               |                |
| 6  | 4                   |          | 30-39, 40-49 |                                    |                 | 2.01E+09 scirpus ariquetar                        | 16.5              | 55              |                       | 0.9          |               | 27.7           |
| 7  | 5                   |          | 50-59        |                                    |                 | 2.01E+09 scirpus ariquetar                        | 5                 | 26.5            |                       |              |               |                |
| 8  | 6                   | 31.46211 | 121.93993    | 70-79                              |                 | 2.01E+09 scirpus ariquetar                        | 11.5              | 24.3            |                       |              |               |                |
| 9  | 7                   | 31.46126 | 121.93273    | 80-89                              |                 | 2.01E+09 scirpus ariquetar                        | 17.5              | 30.4            |                       |              |               |                |
| 10 | 8                   | 31.46034 | 121.93241    | 90-99                              |                 | 2.01E+09 scirpus ariquetar                        | 30                | 21.9            |                       |              |               |                |
| 11 | 9                   | 31.46052 | 121.93196    | 100-109                            |                 | 2.01E+09 phragmites australis & scirpus ariquetar | 30                | 29.1            |                       |              |               |                |
| 12 | 10                  | 31.46092 | 121.93077    | 112-121                            |                 | 2.01E+09 phragmites australis & scirpus ariquetar | 30                | 33.2            |                       |              |               |                |
| 13 | 11                  | 31.46094 | 121.93015    | 122-131                            |                 | 2.01E+09 phragmites australis & scirpus ariquetar | 20                | 28.8            |                       |              |               |                |
| 14 | 12                  | 31.46154 | 121.92883    | 132-141                            |                 | 2.01E+09 scirpus ariquetar                        | 40                | 22.7            |                       |              |               |                |
| 15 | 13                  |          | 142-151      |                                    |                 | 2.01E+09 auidflats                                |                   | 41.4            |                       |              |               |                |
| 16 | 14                  |          | 152-161      |                                    |                 | 2.01E+09 auidflats                                |                   | 42.7            |                       |              |               |                |
| 17 | 15                  | 31.46223 | 121.9278     | 162-171                            | white panel     | phragmites australis & scirpus ariquetar          | 40                | 42.3            |                       |              |               |                |
| 18 | 16                  | 31.46232 | 121.92835    | 182-191                            | disains 182 183 | 2.01E+09 phragmites australis                     | 40                |                 |                       |              |               |                |
| 19 | 17                  | 31.46302 | 121.92626    | 192-201                            |                 | 2.01E+09 phragmites australis                     | 20                | 27.9            |                       |              |               |                |
| 20 | 20160912            |          |              |                                    |                 |   |                   |                 |                       |              |               |                |
| 21 | Point               | Latitude | Longitude    | Spectra Number                     | Text Name       | Vegetation Type                                   | Vegetation Height | (Soil Moisture) | (Vegetation Fraction) | (Wind Speed) | (Temperature) | (Air Humidity) |
| 22 | 1                   | 31.4589  | 121.93537    | 20-39, 47-56                       |                 | scirpus ariquetar                                 | 6                 | 47.6 20-30      |                       | 1.2          |               | 26.6 74.3      |
| 23 | 2                   | 31.45892 | 121.93534    | 58-67, 68-77, 78-87                |                 | scirpus ariquetar                                 | 6                 | 43.6 20-30      |                       | 3.2          |               | 27.6 72.8      |
| 24 | 3                   | 31.459   | 121.93528    | 88-92, 98-107, 108-117, 118-127    |                 | scirpus ariquetar                                 | 6                 | 43.7            |                       |              |               |                |
| 25 | 4                   | 31.46025 | 121.93435    | 221-230, 231-240, 241-249          |                 | scirpus ariquetar                                 |                   | 44.6            |                       |              |               |                |
| 26 | 5                   | 31.46061 | 121.93409    | 251-260, 271-280, 281-290          |                 | scirpus ariquetar                                 | 12                | 40.4            | 70                    | 1.3          |               | 28.4 71.5      |
| 27 | 6                   | 31.46116 | 121.93383    | 291-300, 301-310, 311-320          |                 | phragmites australis & scirpus ariquetar          | 20                | 39.2            | 60                    | 1.5          |               | 28.3 70.4      |
| 28 | 7                   | 31.46176 | 121.93326    | 421-430                            |                 | phragmites australis & raupo                      | 80                | 38.1            | 50                    |              | 1             | 29 66.5        |
| 29 | 8                   | 31.46173 | 121.93326    | 381-390, 391-400                   |                 | phragmites australis & scirpus ariquetar          |                   | 38.9            | 70                    |              |               |                |
| 30 | 9                   | 31.46236 | 121.93312    | 481-490                            |                 | scirpus ariquetar                                 |                   | 36              |                       |              |               |                |
| 31 | 10                  | 31.46278 | 121.9311     | 502-511                            |                 | scirpus ariquetar                                 | 70                | 50.1            | 85                    |              |               |                |
| 32 | 11                  | 31.46132 | 121.92914    | 512-521, 522-530, 531-539          |                 | phragmites australis                              |                   | 33.5            |                       | 1.2          |               | 28.8 61.7      |
| 33 | 12                  | 31.46077 | 121.93103    | 540-550, 551-560, 561-570, 571-580 |                 | phragmites australis                              | 35                | 39.1            | 70                    | 3            |               | 61.2           |
| 34 | 13                  | 31.46057 | 121.93108    | 581-590, 591-600, 601-610          |                 | scirpus ariquetar                                 | 20                | 30.9            | 40                    | 3            |               | 29.3 61.9      |
| 35 | 14                  | 31.45952 | 121.93139    | 611-620, 621-630                   |                 | phragmites australis & scirpus ariquetar          |                   | 38.2            |                       |              |               |                |
| 36 | 15                  | 31.45885 | 121.931      | 631-640, 641-650                   |                 | scirpus ariquetar                                 | 15                | 37.5 60-70      |                       | 3.1          |               | 29.1 60.1      |
| 37 | 16                  | 31.45883 | 121.93068    | 651-660, 661-670                   |                 | scirpus ariquetar                                 | 8                 | 35.6 60-70      |                       | 4            |               |                |

Figure 4 Measurement metadata information

**Figure 5** illustrates the study area, Chongming Dongtan wetlands, sampling locations and measuring dates. I divided the samples (46 points) into four groups according to the date. They are on September 9th to 10th (red points), 12th to 13th (yellow points), 20th to 21st (blue points) and 22nd (purple points).

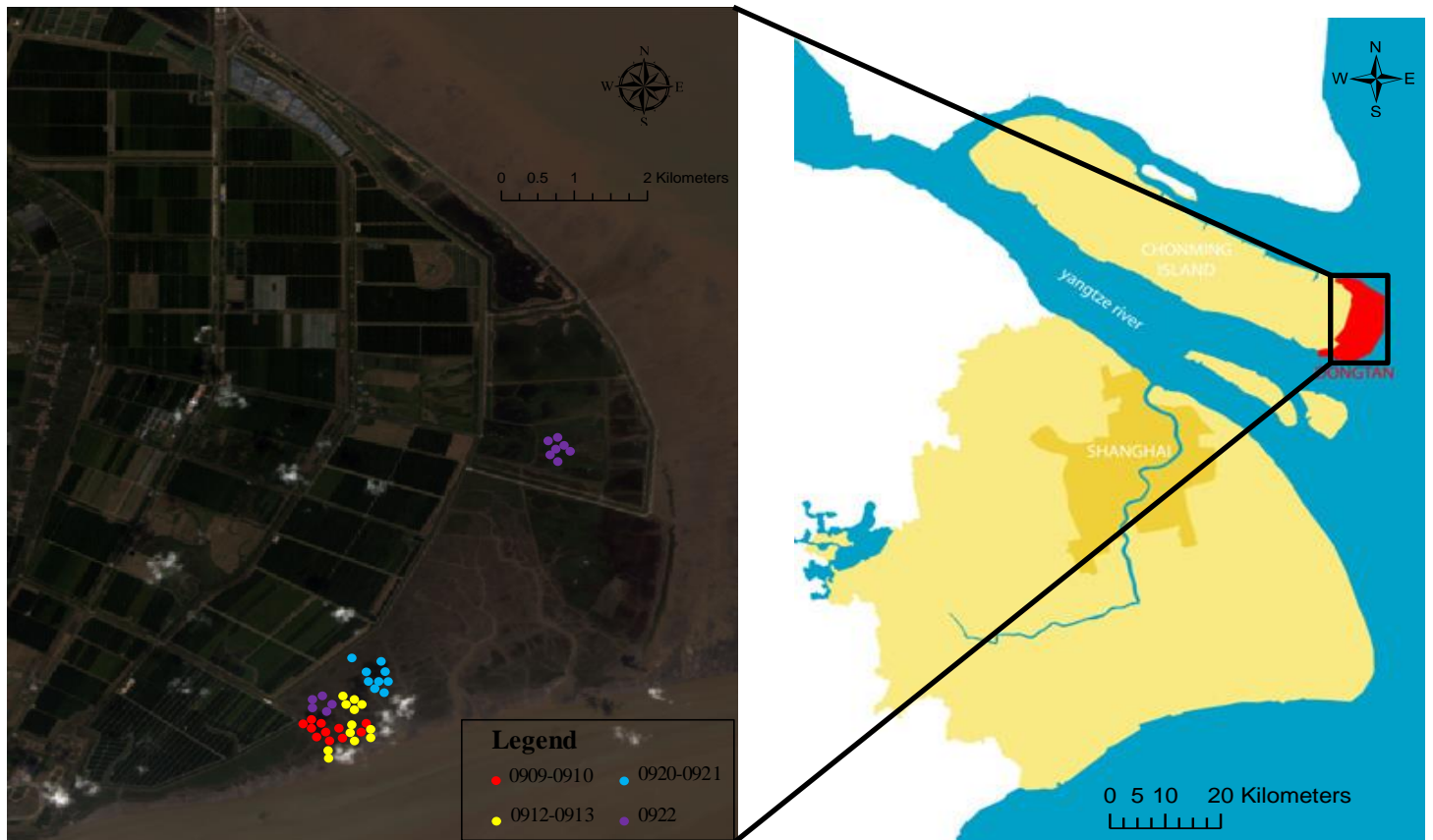


**Figure 5** Landsat 8 image of Chongming Dongtan wetlands on 22nd September, 2016 (band4, 3, 2) and sampling locations and dates

#### ➤ Reflectance spectrum of in situ measurements

The raw reflectance spectral data from FieldSpec handheld 2 (wavelength range 325-1075 nm) can be presented as a reflectance spectrum as **Figure 6 & 7** depict. Average in situ reflectance spectra (5 measurements of reflectance spectra in one place) were obtained through the method of statistical mean calculation abandoning abnormal curves, where a measurement error was obvious.

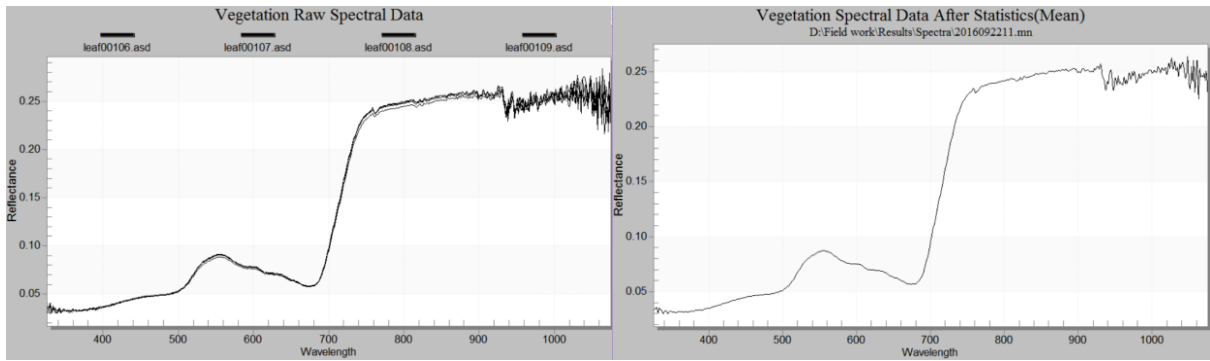


Figure 6 Raw reflectance spectrum of vegetation (left) & spectrum after statistics (right)

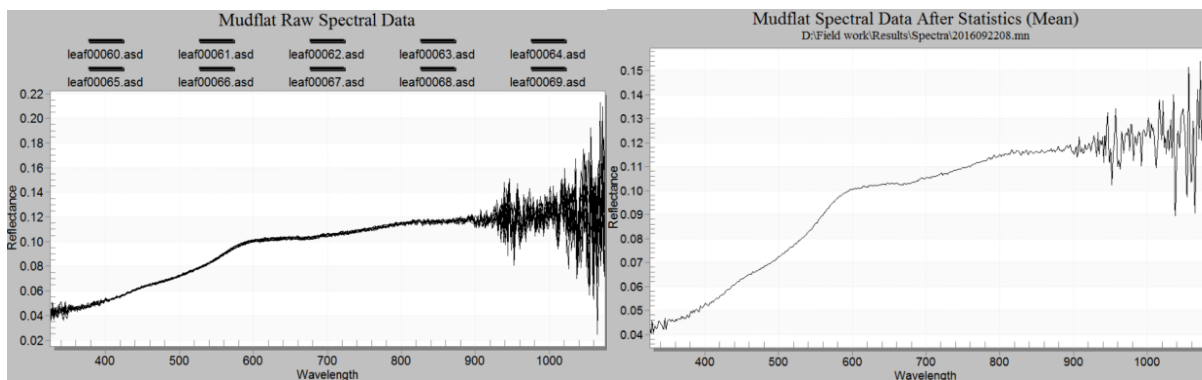
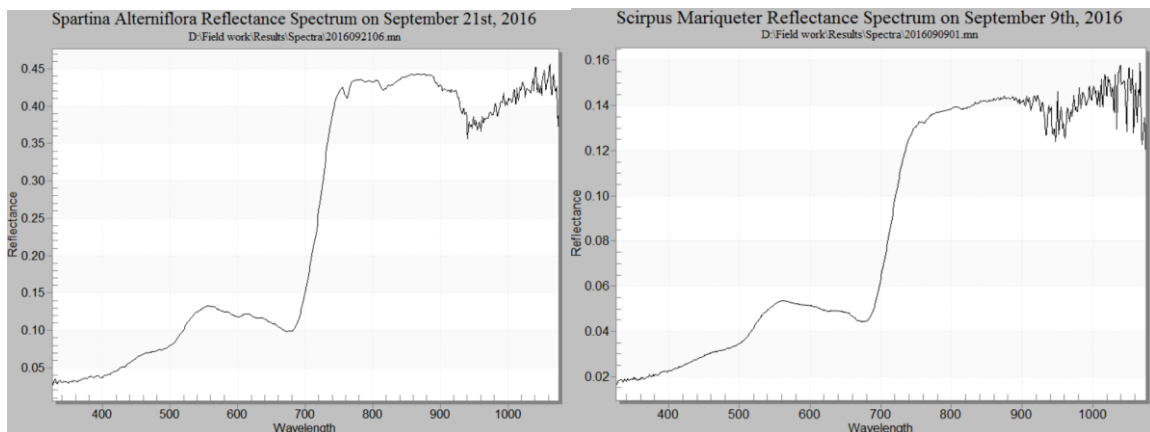


Figure 7 Raw reflectance spectrum of mudflats (left) & spectrum after statistics (right)

As one can see in **Figure 8**, the peak value of *Spartina alterniflora* reflectance spectrum is the highest (0.43), whereas *Phragmites australis* (0.17) is the second and *Scirpus mariqueter* (0.14) is the third. The peak value of mudflats reflectance spectrum is the lowest one (0.13). Meanwhile, the reflectance values of *Scirpus mariqueter* and *Phragmites australis* spectrums are lower than those commonly found for vegetated areas. This may be caused by the dark soil background and low leaf area index.



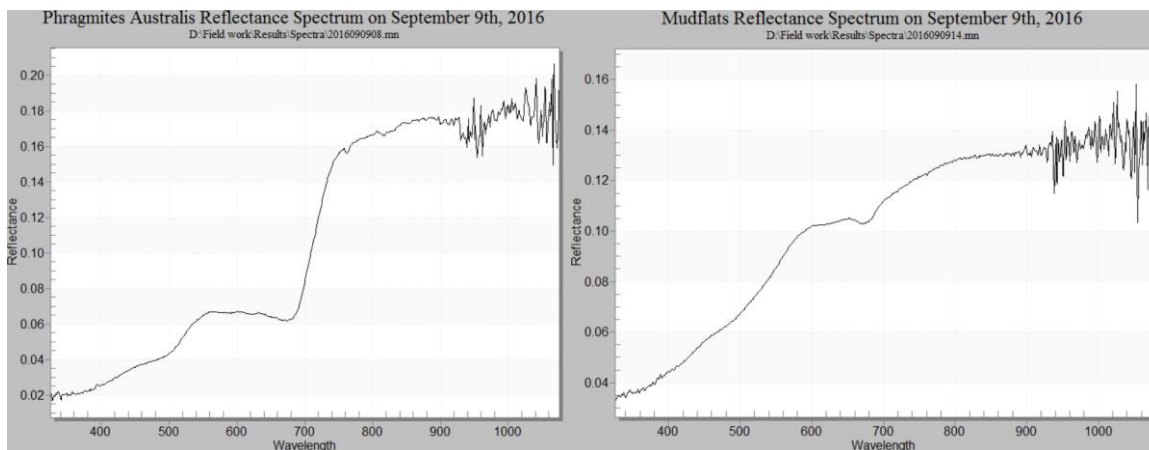


Figure 8 Representative Spectrum of *Spartina alterniflora*, *Scirpus mariqueter*, *Phragmites australis* and mudflats

### 2.2.5. Software & Techniques Support

For field work measuring, ASD FieldSpec handheld 2 (Figure 9) is the main tool for reflectance spectrum collection. Software and techniques used for data preprocessing, statistical analysis and modelling in this study are depicted in Table 3.



Figure 9 ASD FieldSpec handheld 2

Table 3 Software and techniques used in this study

| Software & Techniques      | Application                                 |
|----------------------------|---|
| ILWIS Academic 3.72 & 3.85 | Data preprocessing of images                |
| SCOPE model version 1.61   | Simulation of reflectance, GPP, etc.        |
| Matlab 2016a               | Mapping of vegetation parameters, GPP, etc. |
| Microsoft Word 2010        | Writing thesis                              |
| Microsoft Excel 2010       | Statistical analysis                        |
| Mendeley Version 1.16.1    | Reference processing                        |

|                          |                                 |
|--------------------------|---------------------------------|
| ASD FieldSpec handheld 2 | Reflectance spectrum collection |
|--------------------------|---------------------------------|

### 2.3. Research Methodology

A flowchart illustrating the overall methodology of research can be found as below (**Figure 10**). The main steps include:

- Calibrate the SCOPE model to match in situ reflectance spectra with simulated reflectance spectra from model through adjusting parameter values and obtain the simulated LAI, Cab, GPP, sensible heat flux, latent heat flux and reflectance spectra for sample points.
- Compare the Landsat 8 OLI bands reflectance pixel by pixel with SCOPE simulated reflectance to find a best fit of reflectance for respective pixel and apply Lookup Table approach with the corresponding LAI, Cab, sensible heat flux, GPP and latent heat flux to map of biophysical and biochemical properties.
- Repeat the previous steps with Landsat 5 data and validate the simulated time series of sensible heat flux and latent heat flux with the time series of counterparts collected from flux tower measurements and obtain the final maps.

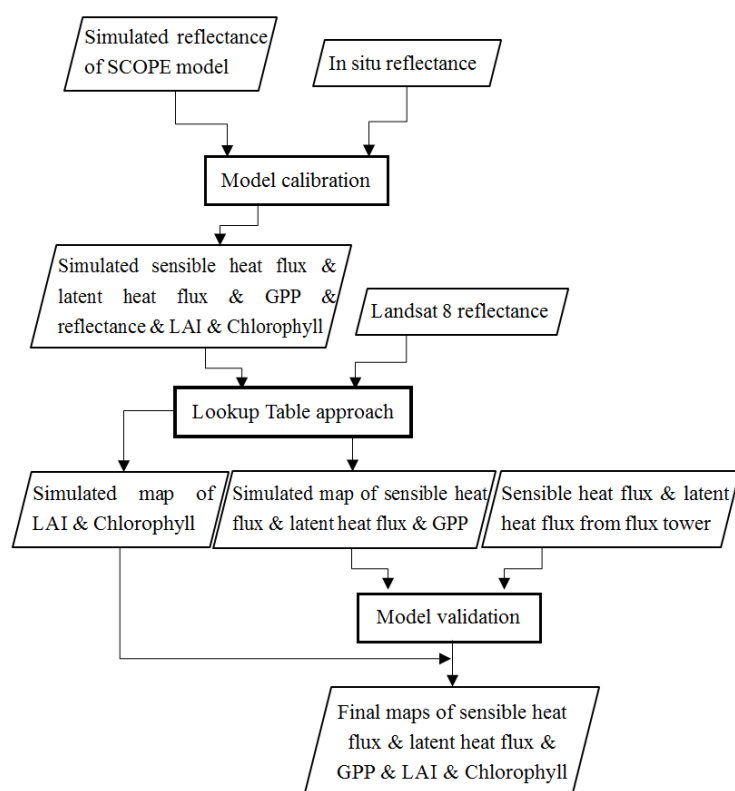


Figure 10 Flowchart of overall methodology in this research

### 2.3.1. Data Pre-processing of Landsat Image

Data preprocessing has been performed to convert the level 1 Landsat 8 image to an atmospherically corrected image with TOC (Top of Canopy) reflectance. To commence with, DN has been converted to reflectance in ILWIS using conversion guidelines and equations provided by USGS ([http://landsat.usgs.gov/Landsat8\\_Using\\_Product.php](http://landsat.usgs.gov/Landsat8_Using_Product.php)), for bands 1 to 9 of Landsat 8 in a subset of the image containing the study area. In addition, atmospheric correction is necessary before retrieving biophysical and biochemical properties such as gross primary productivity (GPP) especially for the visible bands and Near Infrared because they are highly affected by atmospheric scattering. Atmospheric correction has been performed using the SMAC toolbox in ILWIS using the data in **Table 4**. SMAC is a simplification of the Code 6s (RAHMAN & DEDIEU, 1994) for AC of visible and near visible bands of some satellite sensors. According to the methodology of SCOPE model simulation, the TOC (top of canopy) reflectance of each band of Landsat images is crucial to the results of simulations. Therefore, it's necessary to carry out the atmospheric correction process as accurate as possible to obtain the satisfying final results.

**Table 4 Necessary parameters and their data source of Atmospheric Correction**

| No. | Input Data for SMAC       | Unit              | Data Source                    |
|-----|---------------------------|-------------------|--------------------------------|
| 1.  | Aerosol Optical Thickness | —                 | AERONET Website                |
| 2.  | Water Vapor               | g/cm <sup>2</sup> | AERONET Website                |
| 3.  | Ozone                     | g.atm.cm          | Ozone & Air Quality Website    |
| 4.  | Surface Pressure          | hpa               | Chinese Meteorological Station |
| 5.  | Solar Azimuth             | degrees           | Landsat Image Products         |
| 6.  | Solar Zenith              | degrees           | Landsat Image Products         |
| 7.  | Sensor Zenith             | degrees           | Assumed NADIR                  |
| 8.  | Sensor Azimuth            | degrees           | 0                              |

### 2.3.2. Model Calibration with In Situ Data

The process of model calibration is illustrated as **Figure 11**. RTMo is the radiative transfer part of SCOPE for the VNIR (visible to near infrared) (Christiaan Van Der Tol et al., 2016). It is a version of SAIL (Scattering by Arbitrary Inclined Leaves) which is one of the earliest canopy reflectance models (Jacquemoud et al., 2009) with a soil reflectance model. After inputting the In situ reflectance from field sampling into the RTMo retrievals of SCOPE model, the best estimates of vegetation and soil parameters

were obtained. Meanwhile, the simulated reflectance spectra are also obtained. In order to reach the optimization of parameter sets, Objective Function (**Equation 1**) has been selected to evaluate the results of the model calibration. The tools for the best fitting are already available (<https://github.com/christiaanvandertol>). Subsequently, the retrieved parameters (Cab, LAI and soil parameters, etc.) are obtained.

The Objective Function used for the retrieval was:

$$RMSE\ 1 = \sqrt{\sum_{i=1}^n \frac{(Simulated\ reflectance - In\ situ\ reflectance)^2}{n}} \quad [1]$$

Where RMSE 1 is the root mean square error between simulated reflectance and in situ reflectance,  $n$  is the number of bands of in situ reflectance spectra, the simulated reflectance is the output reflectance of SCOPE model and the in situ reflectance is the measured reflectance in the field.

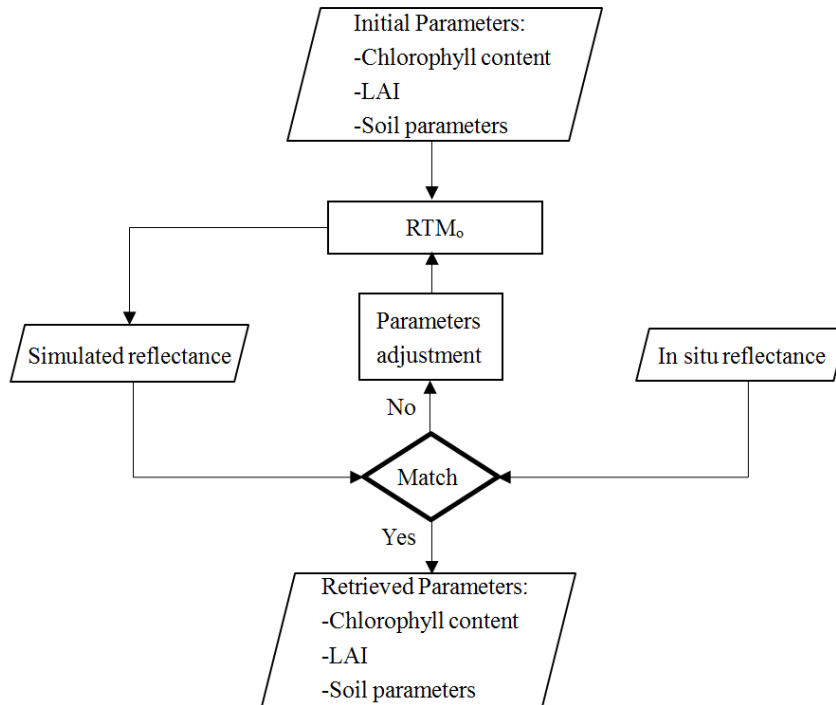


Figure 11 Flowchart of model calibration process in this research

### 2.3.3. Simulated Maps from SCOPE Model with Landsat 8 Data

The SCOPE model simulated productivity and sensible heat flux, latent heat flux corresponds to respective reflectance data obtained based on iterative calculation of SCOPE algorithm. By using

reflectance data and corresponding meteorological data, the productivity, sensible heat flux and latent heat flux can be simulated by SCOPE model calibration, it is possible to estimate productivity, sensible heat flux and latent heat flux from for example a Landsat 8 image.

The process of this step is illustrated as **Figure 12**. With the retrieved parameters from **Chapter 2.3.2**, the full SCOPE model was run to obtain simulated reflectance spectra, sensible heat flux, latent heat flux, productivity of the vegetation with the retrieved LAI and chlorophyll content. The next stage is to convert simulated reflectance after calibration into Landsat 8 OLI bands (**Table 1**) through Matlab programming. Moreover, to infer the sensible heat flux, productivity and latent heat flux of Landsat 8 OLI imagery, it is necessary to compare the Landsat 8 OLI bands reflectance pixel by pixel with SCOPE simulated reflectance and to find a best fit of reflectance for the respective pixel. To achieve this, the lookup table approach (LUT) was adopted. For finding best fit of simulated reflectance from a lookup table for given Landsat 8 OLI pixels, Equation 2 is used as cost function. The code finds the best matching reflectance from the table of simulated reflectance from Landsat 8 OLI per pixel, and put them into row and columns and translates the Landsat image into SCOPE model output image. The simulated maps of sensible heat flux, latent heat flux, productivity and corresponding LAI and chlorophyll content can be obtained in this way.

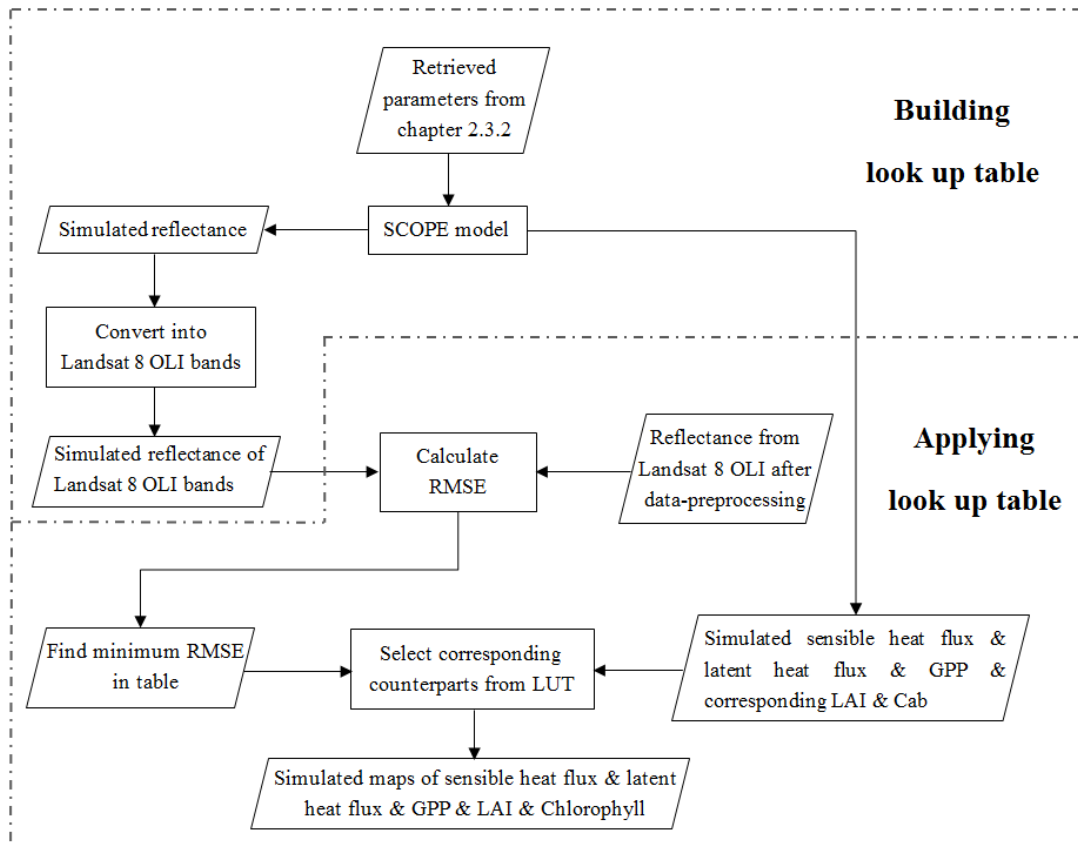


Figure 12 Flowchart of the Lookup Table approach in this research

$$RMSE\ 2 = \sqrt{\sum_{i=1}^n \frac{(Simulated\ reflectance - Landsat8\ reflectance)^2}{n}} \quad [2]$$

Where RMSE 2 is the root mean square error between simulated reflectance and Landsat 8 reflectance,  $n$  is the number of bands of Landsat 8 image, Simulated reflectance is the output reflectance of SCOPE model converting into Landsat 8 OLI bands (the first seven bands) after calibration and Landsat 8 reflectance is the TOC reflectance from Landsat 8 OLI image.

### 2.3.4. Model Validation

The process of this step is illustrated as **Figure 13**. I did not have GPP processed (only NEE) from flux tower data, and therefore limited to sensible heat flux and latent heat flux for model validation. First of all, it's necessary to repeat the steps in **Chapter 2.3.3** to get the simulations of sensible heat flux, latent heat flux and the corresponding soil spectra, LAI and chlorophyll content in the year from 2005 to 2007 using Landsat 5 images. Meanwhile, soil spectra, LAI & chlorophyll around flux tower from simulations can be selected through the above simulations. Then, the time series of sensible heat flux and latent heat flux were simulated with the time series module of SCOPE model with the value of the above soil spectra, LAI & chlorophyll around the flux tower.

Furthermore, the measured time series of sensible heat flux and latent heat flux were compared to field measurements (The flux tower data for the year from 2005 to 2007 was available at SKLEC). Then model validation was carried out through comparing the two curves mentioned above using Objective Function (Equation 3).

$$RMSE\ 3 = \sqrt{\sum_{i=1}^n \frac{(Simulated\ results - Flux\ tower\ data)^2}{n}} \quad [3]$$

Where RMSE 3 is the root mean square error between simulated results and flux tower data,  $n$  is the number of measuring records, simulated results include the sensible heat flux, productivity and latent heat flux from time series module of SCOPE model in the year from 2005 to 2007 using Landsat 5 TM images and Flux tower data is the corresponding sensible heat flux, productivity and latent heat flux collected from 2005 to 2007 at SKLEC.

Finally, after validation for 2005 to 2007, the final maps of sensible heat flux, latent heat flux, productivity and corresponding LAI and chlorophyll content in 2016 have been obtained.

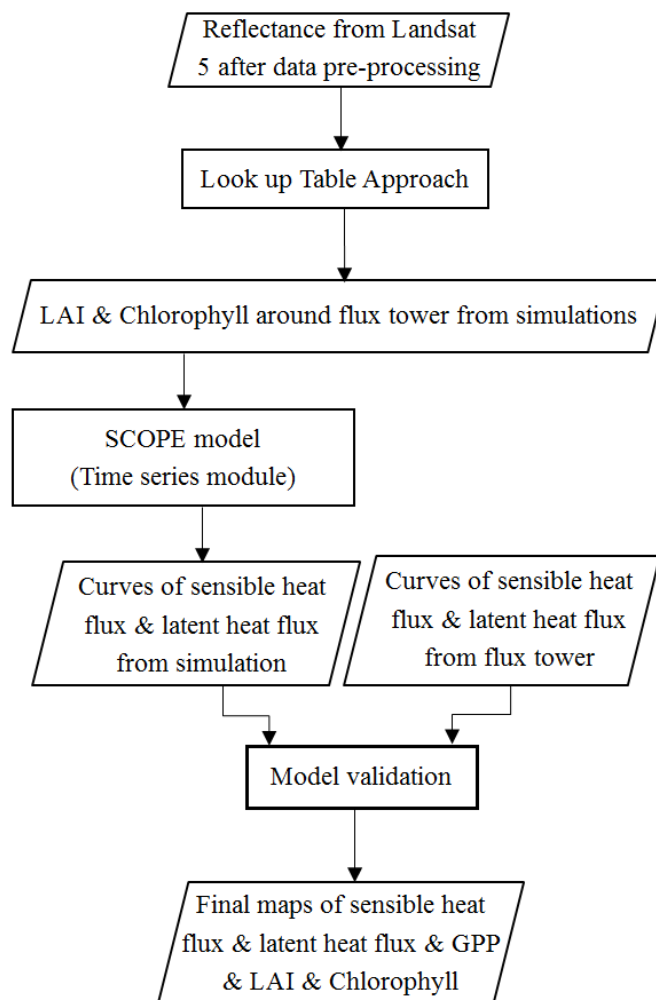


Figure 13 Flowchart of model validation process in this research

### 3. RESULTS

#### 3.1. Results of Atmospheric Correction for Landsat images using ILWIS SMAC Toolbox

Due to the significance of atmospheric correction of images, this section describes the detailed data source and data selection for the AC (atmospheric correction) process in detail. Meanwhile, it also describes the results of TOC reflectance which are regarded as the input materials of Matlab compiling for applying look up table approach after AC process.

This section using Landsat 8 OLI image at 2:25 on 22<sup>nd</sup> September in 2016 as an example shows the results, and processing procedure of Landsat 5 TM images are similar.

##### 3.1.1. Input Data of SMAC Toolbox in ILWIS

Taihu station (31°25'15" N, 120°12'54" E) was chosen as atmospheric measurement site for collecting the values of AOT (aerosol optical thickness) and water vapor in my study area as **Figure 14 & Figure 15** shown. Due to the lack of data, the 3<sup>rd</sup> of September in 2016 as used to obtain the AOT value at 550nm. The ozone value was selected by **Figure 16** and surface pressure on September in 2016 was collected in Baoshan meteorological station. As for the solar azimuth and solar zenith were both from head information of Landsat 8 OLI image product. The final input data of SMAC is described in **Table5**.

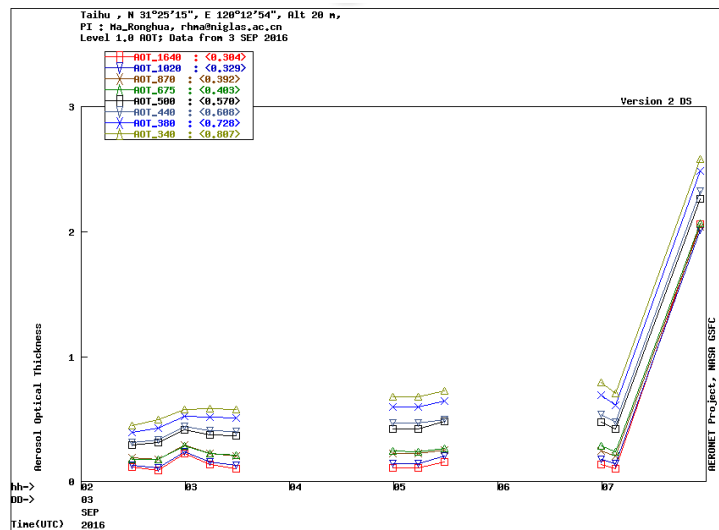


Figure 14 AOT of Taihu station on 3<sup>rd</sup> September in 2016

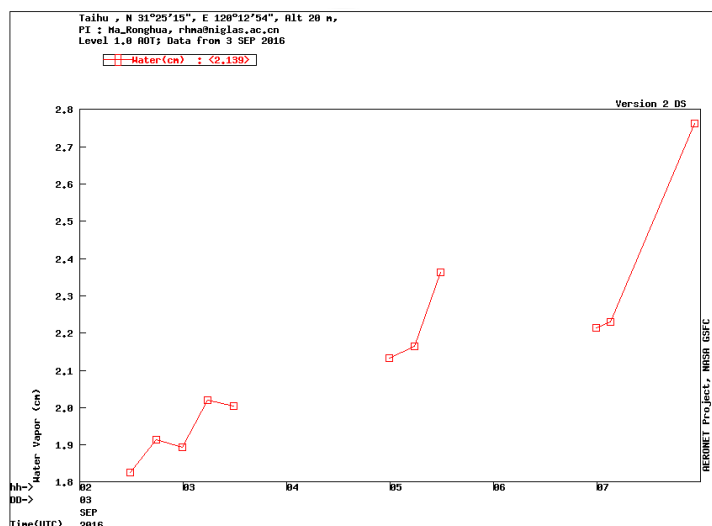


Figure 15 Water vapor of Taihu station on 3<sup>rd</sup> September in 2016

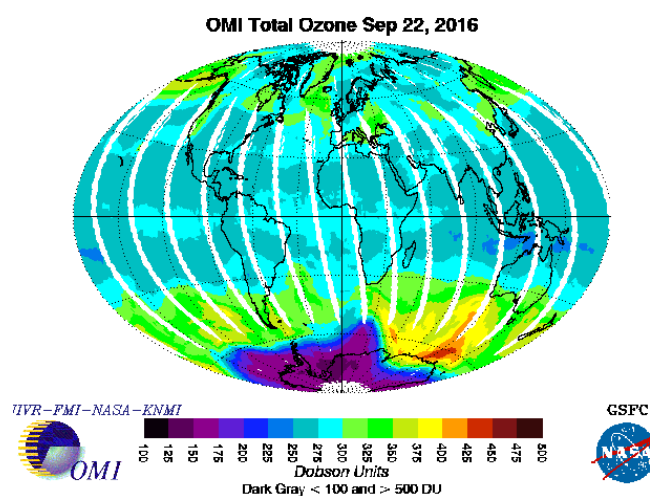


Figure 16 Total ozone map on 22<sup>nd</sup> September in 2016

Table 5 The final input data of SMAC

| No. | Input Data for SMAC       | Unit              | Data Source |
|-----|---------------------------|-------------------|-------------|
| 1.  | Aerosol Optical Thickness | —                 | 0.3106      |
| 2.  | Water Vapor               | g/cm <sup>2</sup> | 1.83        |
| 3.  | Ozone                     | g.atm.cm          | 0.2875      |
| 4.  | Surface Pressure          | hpa               | 1012.9      |
| 5.  | Solar Azimuth             | degrees           | 145.294     |
| 6.  | Solar Zenith              | degrees           | 36.742      |
| 7.  | Sensor Zenith             | degrees           | 0           |

---

|    |                |         |   |
|----|----------------|---------|---|
| 8. | Sensor Azimuth | degrees | 0 |
|----|----------------|---------|---|

---

### 3.1.2. Results of TOC Reflectance after AC Process

**Figure 17** shows the TOC reflectance after AC in natural color composite using the scripts in ILWIS software with the above input data. There were still some clouds existing over the study area in the image. Before converting the TOC reflectance of the first 7 bands of Landsat 8 OLI image into the text format as the input materials of Matlab compiling for applying look up table approach, the quality of the AC was verified by selecting an ocean reflectance spectrum (**Figure 18 (a)**) as the reference to check TOC reflectance of the first 7 bands of Landsat 8 OLI image. I selected one pixel (31°4'48.49" N, 122°2'57.59" E) of the ocean part in the image and illustrated the reflectance spectra of that pixel of the first 7 bands of Landsat 8 in **Figure 18 (b)**. Comparing the two figures, the final results of TOC reflectance after AC process are satisfactory.



**Figure 17** TOC reflectance after AC of Landsat 8 image in Dongtan on September 22<sup>nd</sup>, 2016 (band4, 3, 2)

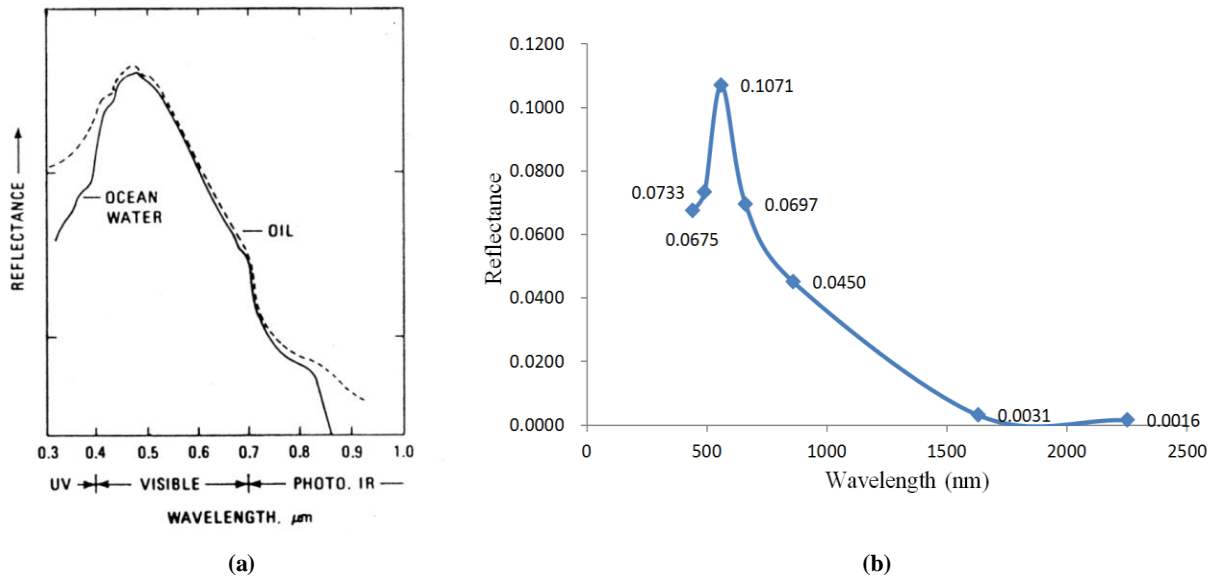


Figure 18 (a) The ocean reflectance spectrum (M.J.A. Butler et al., 1988); (b) The reflectance spectra of one pixel of the first 7 bands of Landsat 8 in the ocean part after atmospheric correction

### 3.2. Results & Analysis of Model Calibration with Measurements and Simulations

The objective of this section is to calibrate the measuring data with the simulation ones to select the best vegetation parameters as the input data in SCOPE model simulations through adjusting parameter values with some prior information (Lin & Chen, 2009; Zhong et al., 2016).

#### 3.2.1. Mudflats

RTMo (transfer of solar and sky radiation) retrievals of SCOPE model should be used for this section. For the mudflats, the LAI was set to zero (no vegetation), and then the soil parameters (soil brightness (B), parameters that determine the shape of the soil reflectance spectrum excluding soil brightness (lat and lon) and soil moisture content (SMp) which mostly affects the soil brightness) are varied to obtain the optimization of soil parameters and simulations for each sample points (**Figure 19**). As all the 15 graphs of mudflats spectrums shown, the measurements matched the simulations pretty well. Especially, the total one (**Figure 20**) that represented the RTMo results and measured data was fairly satisfying excluding the final noise (reflectance after 900nm). Meanwhile, the RMSE values between the simulations and measuring data for each sample point are all below 0.014, and its mean value is 0.00524 (**Figure 21**). The calibration of soil parameters can be accepted.

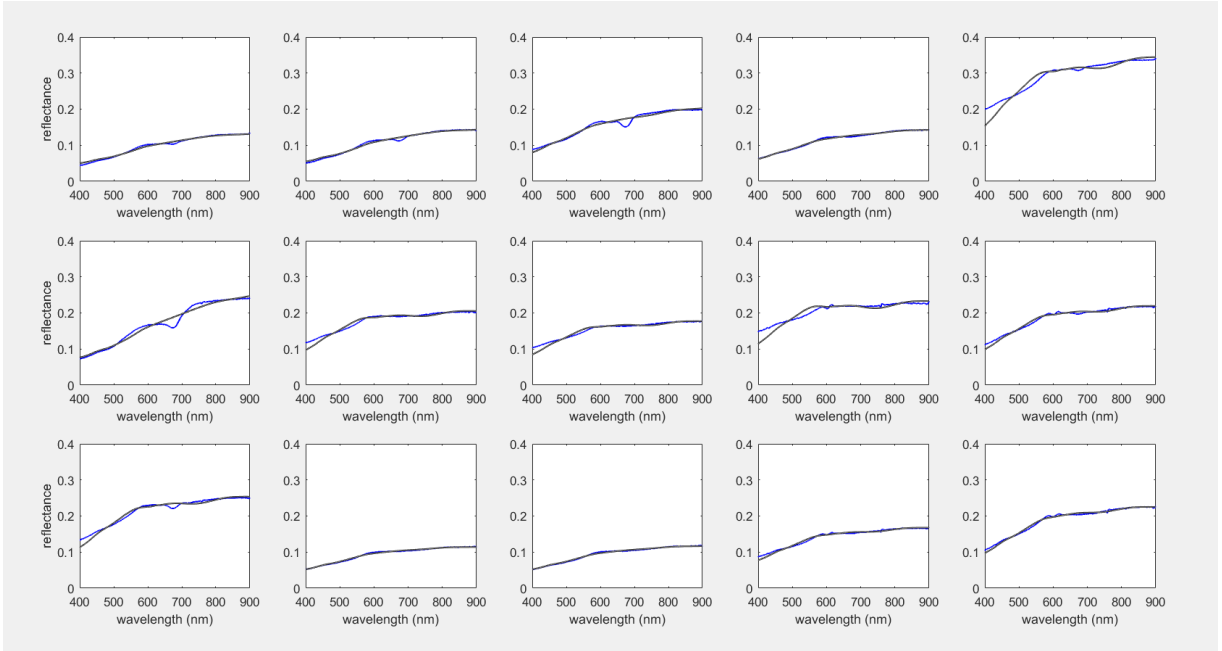


Figure 19 The simulated (gray line) and measuring (blue line) reflectance spectrums of mudflats in each sample point

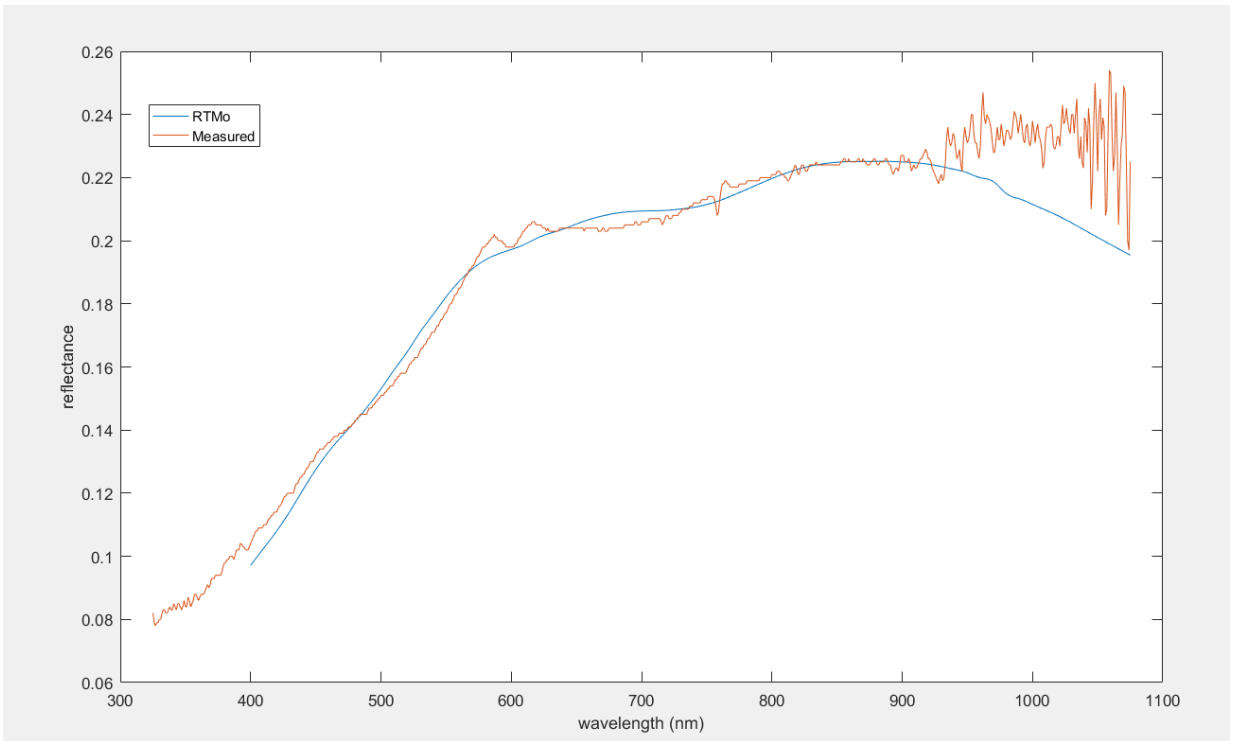


Figure 20 The total simulated and measuring reflectance spectrums of mudflats

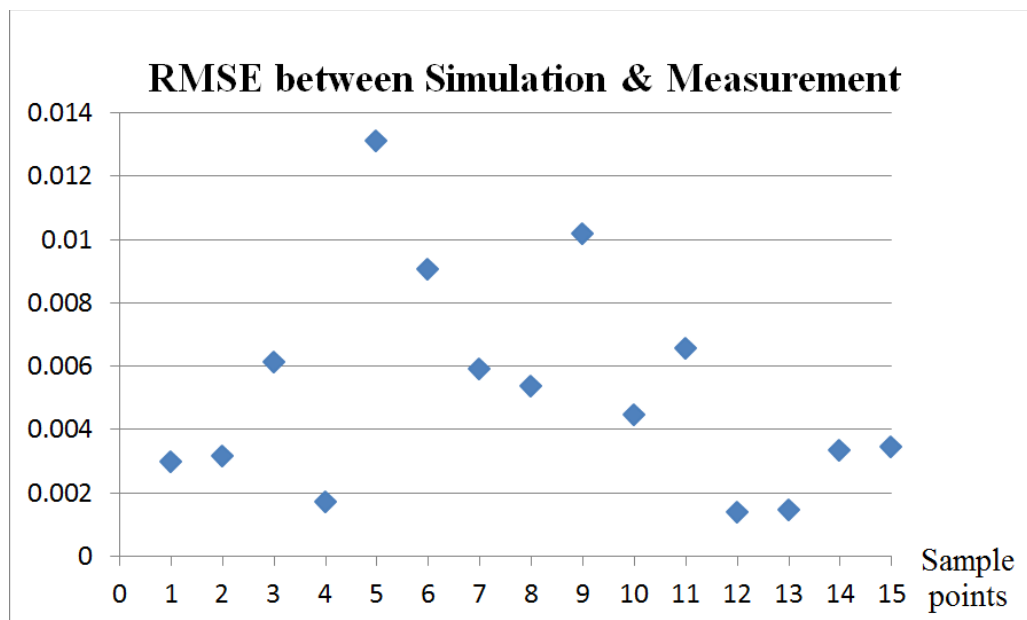


Figure 21 The RMSE value between simulations & measurements of mudflats in each sample point

Table 6 depicts the maximum, minimum and mean values of those 4 soil parameters after simulations of RTMo retrievals. I selected the mean values of those 4 soil parameters as the soil basic values in RTMo retrievals of SCOPE model.

Table 6 The maximum, minimum and mean values of 4 soil parameters in RTMo retrievals

| Parameters | Maximum | Minimum | Mean    |
|------------|---------|---------|---------|
| B          | 0.8187  | 0.3042  | 0.5354  |
| lat        | 28.7078 | 23.2313 | 26.9000 |
| lon        | 44.8608 | 17.5263 | 29.8265 |
| SMp        | 51.4208 | 14.7901 | 43.1477 |

### 3.2.2. Vegetation

Based on the above results of mudflats, 4 soil parameters were treated as constant for the vegetated areas and the vegetation parameters (the chlorophyll concentration of the leaves (Cab), the carotenoid concentration of the leaves (Cca), dry matter concentration of the leaves (Cmd), the water concentration of the leaves (Cw), senescent material content (Cs), the mesophyll thickness parameter (N), determines the leaf inclination parameter (LIDFa), determines the bimodality of the leaf inclination (LIDFb), and the leaf area index (LAI)) were retrieved. According to the types of vegetation (*Phragmites australis*, *Scirpus mariqueter* and *Spartina alterniflora*), simulations of vegetation parameters were divided into three parts as Figure 22

describes. All of them were quite satisfying due to the fact that the simulations matched measurements quite well in the wavelength range between 400 nm and 900nm. As for the value of RMSE between simulations and measurements, *Phragmites australis* is no more than 0.004, *Scirpus mariqueter* is no more than 0.005 and *Spartina alterniflora* is no more than 0.008. Thus, the spectra were well reproduced after the calibration. However, independent leaf measurements were available to validate whether the retrieved parameters were correct.

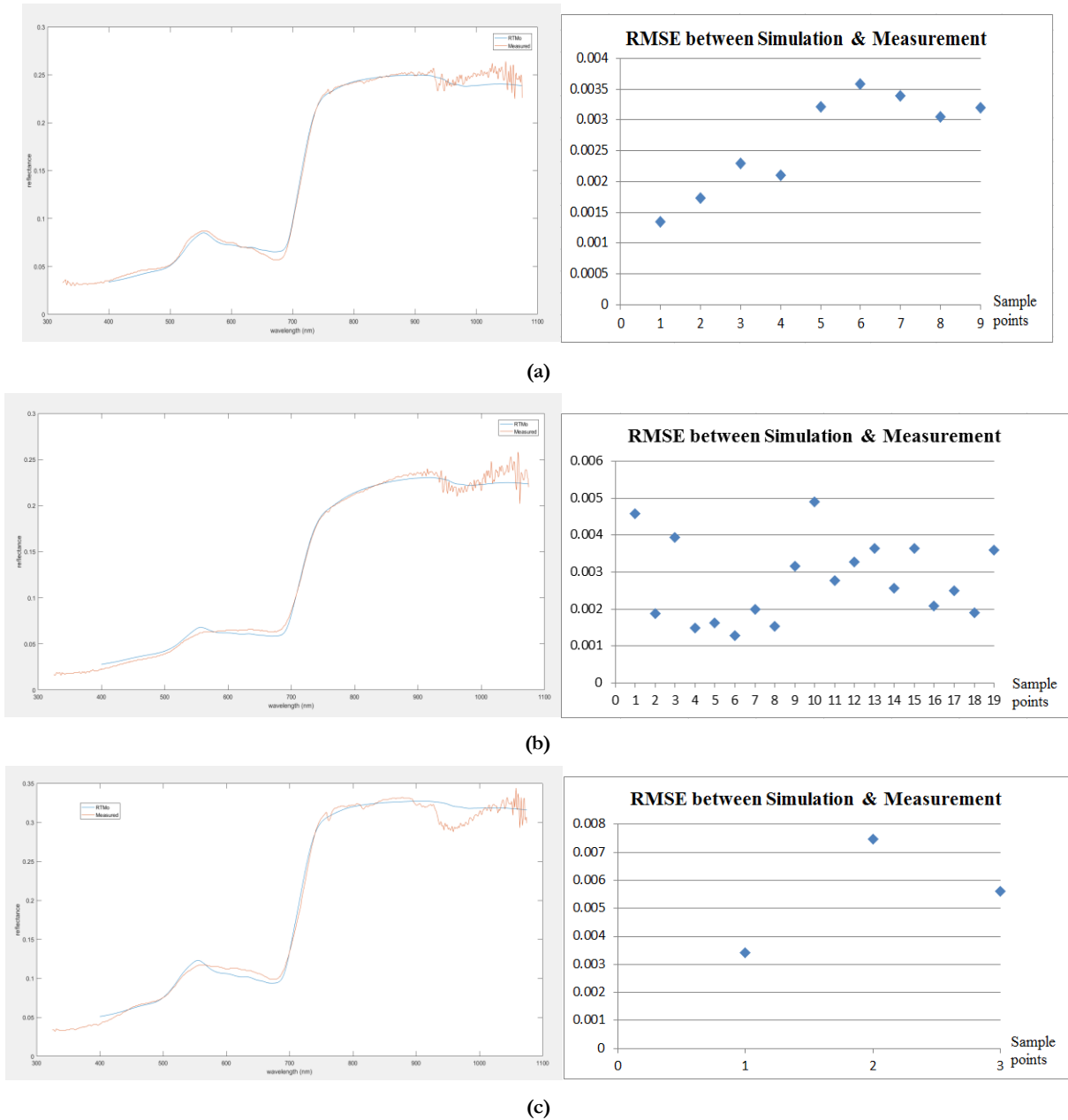


Figure 22 The total curves and RMSE value between simulations & measurements of three vegetation types: (a) *Phragmites australis*, (b) *Scirpus mariqueter*, (c) *Spartina alterniflora*

**Table 7** illustrates the maximum, minimum and mean values of 9 vegetation parameters for 3 vegetation types after retrievals using RTMo. The mean values of 6 vegetation parameters (Cmd, Cw, Cs, N, LIDFa, LIDFb) for 3 vegetation types and the mean values of the above 4 soil parameters (B, lat, lon and SMp) were selected as the input data in the next step of SCOPE model simulation: the generation of the lookup table for retrievals from Landsat 8.

**Table 7 The maximum, minimum and mean values of 9 vegetation parameters for 3 vegetation types in RTMo retrievals**

| Parameters                         | <i>Phragmites Australis</i> |         |         | <i>Scirpus Mariqueter</i> |         |         | <i>Spartina Alterniflora</i> |         |         |
|------------------------------------|-----------------------------|---------|---------|---------------------------|---------|---------|------------------------------|---------|---------|
|                                    | Maximum                     | Minimum | Mean    | Maximum                   | Minimum | Mean    | Maximum                      | Minimum | Mean    |
| Cab ( $\mu\text{g cm}^{-2}$ )      | 56                          | 21      | 31.     | 59                        | 15      | 29      | 59                           | 37      | 52      |
| Cw ( $\text{g cm}^{-2}$ )          | 0.0213                      | 0.0152  | 0.0184  | 0.0322                    | 0.0159  | 0.0228  | 0.0180                       | 0.0135  | 0.0151  |
| Cmd ( $\text{g cm}^{-2}$ )         | 0.0121                      | 0.0002  | 0.0059  | 0.0200                    | 0.0002  | 0.0132  | 0.0069                       | 0.0001  | 0.0024  |
| Cs (a. u)                          | 0.3073                      | 0.0601  | 0.2000  | 0.3996                    | 0.0128  | 0.2258  | 0.2105                       | 0.0850  | 0.1288  |
| Cca ( $\mu\text{g cm}^{-2}$ )      | 10.5                        | 6.2     | 8.6     | 11.4                      | 7.4     | 9.4     | 13.7                         | 9.2     | 11.7    |
| N (dimensionless)                  | 2.27                        | 1.06    | 1.45    | 2.07                      | 1.00    | 1.17    | 3.46                         | 1.50    | 2.78    |
| LAI ( $\text{m}^2 \text{m}^{-2}$ ) | 1.56                        | 0.99    | 1.35    | 2.38                      | 0.34    | 1.74    | 2.51                         | 0.43    | 1.23    |
| LIDFa                              | -0.1401                     | -0.9802 | -0.7128 | 0.0788                    | -1.0000 | -0.8820 | 0.7117                       | -0.5570 | 0.2272  |
| LIDFb                              | -0.0048                     | -0.1637 | -0.1130 | 0.0068                    | -0.1283 | -0.0321 | -0.0518                      | -0.1337 | -0.0821 |

### 3.3. Mapping of Productivity, Latent Heat Flux, Sensible Heat Flux and Vegetation parameters (LAI & Chlorophyll)

#### 3.3.1. Input Data Selection of SCOPE Model Simulation

After atmospheric correction, due to the fact that the reflectance from Landsat 8 OLI image is not sensitive to the meteorological conditions, it's not necessary to include more than one value for the meteorological conditions in the LUT. The fluxes were calculated for just one example of meteorological conditions as illustrated in **Table 8**. First of all, three vegetation parameters (Cab, Cca and LAI) were selected as variable value to be included in the LUT due to the fact that LAI and Chlorophyll are much more sensitive to the simulation and the others as default to carry out Look-up table simulation in SCOPE model. The values selection of Cab, Cca, soil spectra (5representative soil spectra of measurements were selected for SCOPE simulation) and LAI are described in **Table 9**.

**Table 8** The meteorological conditions used for the simulation of fluxes in the LUT

| Meteorological Parameters | Value | Units             |
|---------------------------|-------|-------------------|
| z                         | 10    | m                 |
| Rin                       | 600   | W m <sup>-2</sup> |
| Ta                        | 20    | T                 |
| Rli                       | 300   | W m <sup>-2</sup> |
| p                         | 970   | hPa               |
| ea                        | 15    | hPa               |
| u                         | 2     | m s <sup>-1</sup> |
| Ca                        | 380   | ppm               |
| Oa                        | 209   | per mille         |

**Table 9** The values selection of Cab, Cca and LAI in SCOPE model input data

| Parameter               | Value Selection |     |     |     |     | Count |
|-------------------------|-----------------|-----|-----|-----|-----|-------|
| Cab                     | 0               | 2   | 4   | ... | 60  | 31    |
| Cca                     | 0               | 4   | 8   | 12  | 14  | 5     |
| Soil spectrum<br>number | 2               | 5   | 6   | 9   | 12  | 5     |
| LAI                     | 0               | 0.2 | 0.4 | ... | 2.6 | 14    |

\* Soil spectrum number refers to a retrieved soil spectrum from the measurements that were provided in the LUT.

### 3.3.2. Results of Simulated Reflectance from SCOPE Model

Based on the above input data, a total number of 6045 simulated reflectance spectra, productivity, latent heat flux and sensible heat flux from all combinations of input parameters were obtained. Example for a number of spectra is illustrated in **Figure 23**. The grey lines represent the simulated reflectance spectra of SCOPE model and the black points show the values integrated over (**Figure 24**) Landsat 8 OLI first seven bands (based on **Table 1**). For the purpose of this research however, only the SCOPE model simulated reflectance in Landsat 8's seven spectral bands is required. Therefore, it is necessary to extract reflectance from SCOPE simulated reflectance spectrums that correspond to Landsat 8 OLI bands as shown in **Figure 25**.

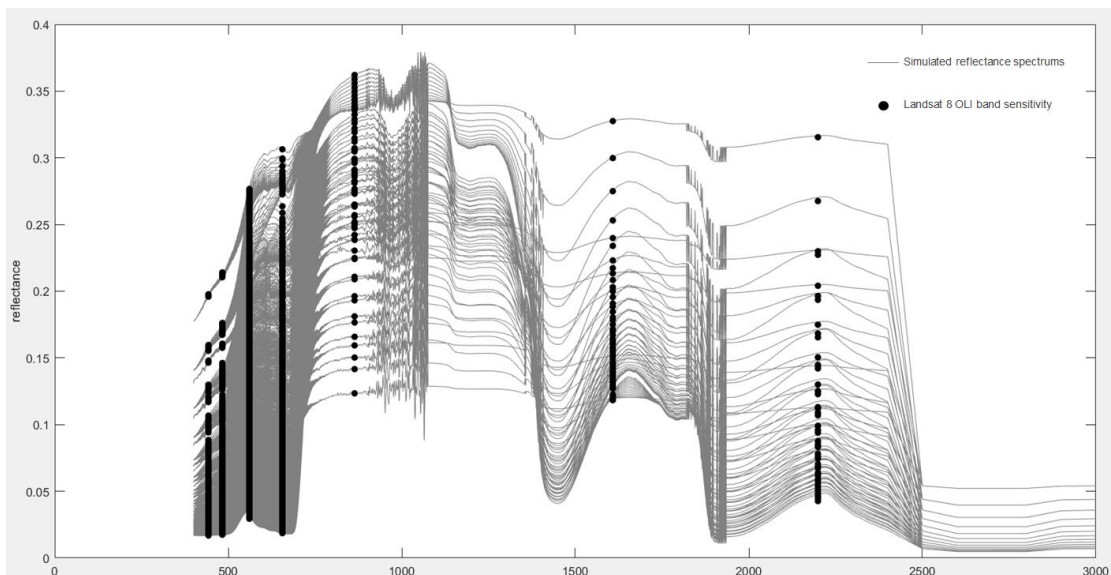


Figure 23 The simulated reflectance spectrums corresponding to Landsat 8 OLI band sensitivity

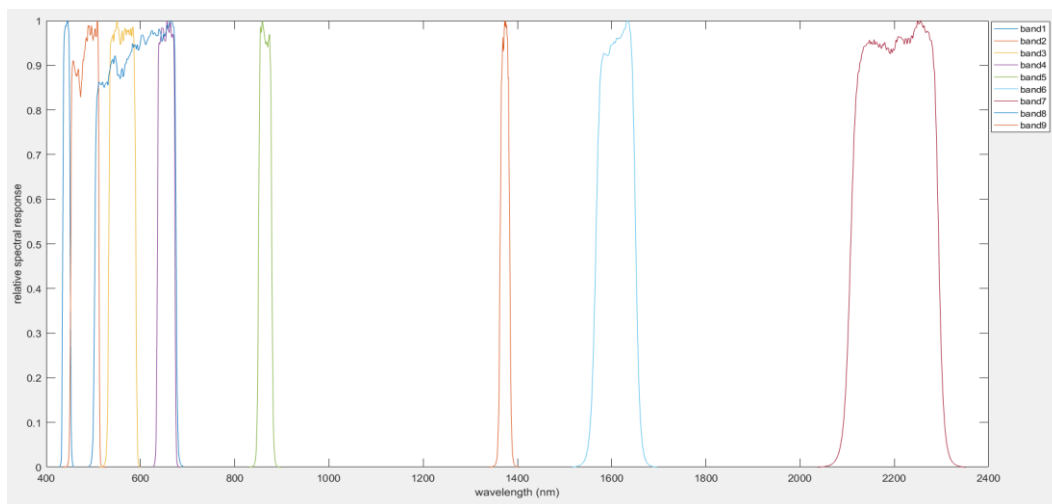


Figure 24 Landsat 8 OLI band sensitivity

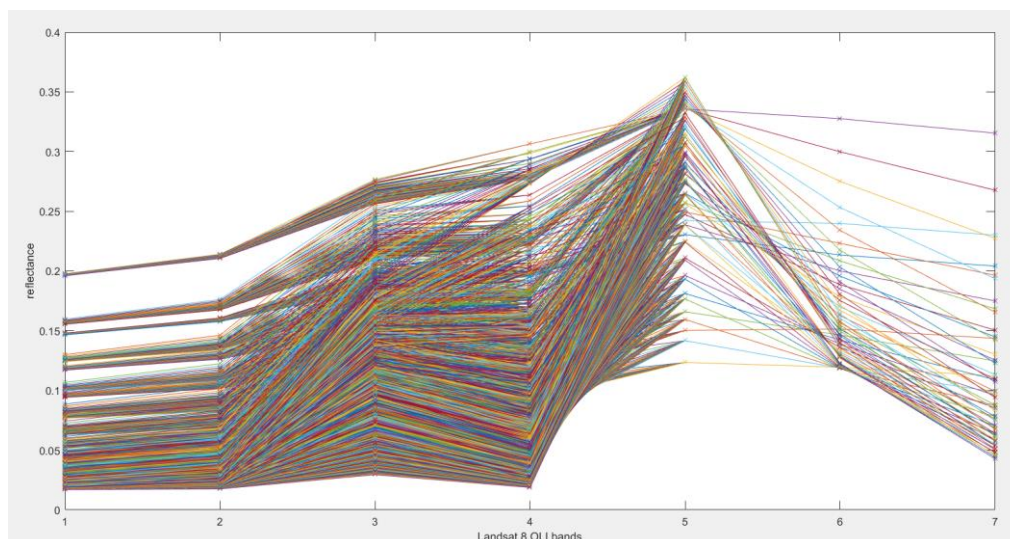


Figure 25 Spectra of SCOPE simulated reflectance's extracted only in Landsat 8 first seven bands

### 3.3.3. Maps & Analysis of Productivity, Latent Heat Flux, Sensible Heat Flux and Vegetation parameters (LAI & Chlorophyll)

Based on the above simulated reflectance spectra and the results of **chapter 3.1**, simulated maps of productivity, latent heat flux, sensible heat flux and vegetation parameters (LAI & Cab) were obtained by minimizing Equation 2 for each Landsat 8 pixel Matlab. As seen from **Figure 26**, RMSE value of the ocean part is relatively high (around 0.08), and also RMSE value of some clouds in the map reach 0.20. This is obviously because the SCOPE simulates the land surface well, but not the ocean. Therefore, due to the accuracy of my simulated results, all retrieved data where  $RMSE > 0.05$  were masked, and in the maps for chlorophyll (Cab), LAI, productivity, latent heat flux and sensible heat flux shown in **Figure 27**, **Figure 28**, **Figure 29**, **Figure 30** and **Figure 31** respectively.

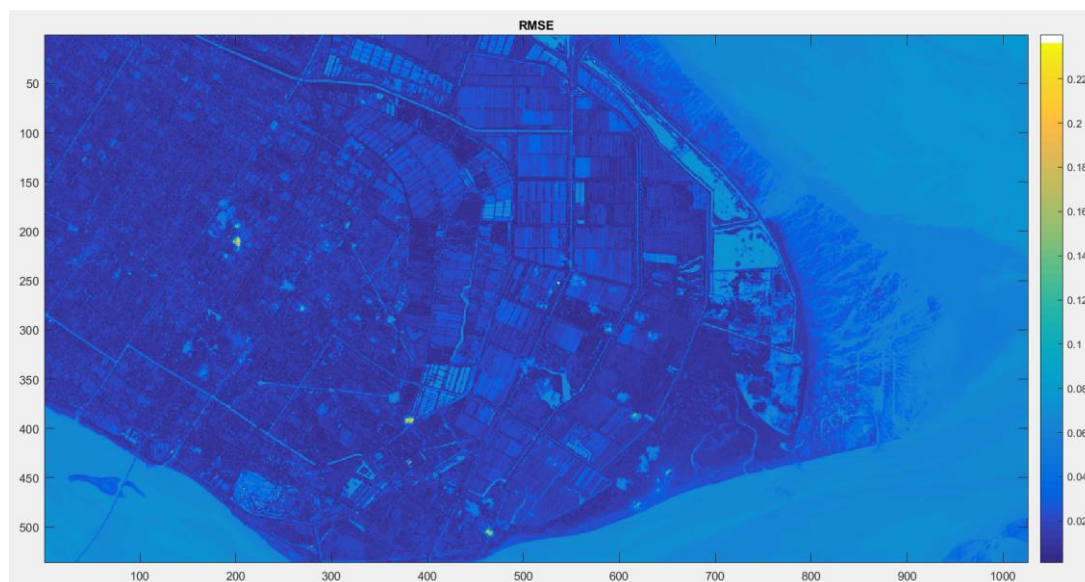


Figure 26 Map of RMSE between models simulated reflectance and Landsat 8 OLI pixel reflectance in Chongming Dongtan

As we can see from Figure 27, chlorophyll pigment concentration in coastal tidal wetlands in image is between  $5 \mu\text{g cm}^{-2}$  and  $60 \mu\text{g cm}^{-2}$  and those who have higher concentration are resembles to agriculture farms or parks in the whole map. Meanwhile, chlorophyll concentration in urban area is less than  $10 \mu\text{g cm}^{-2}$ . As for the masked part in chlorophyll map, it represents the masked area of which  $\text{RMSE} > 0.05$ . The reasons for the strange phenomenon can be explained in discussion chapter.

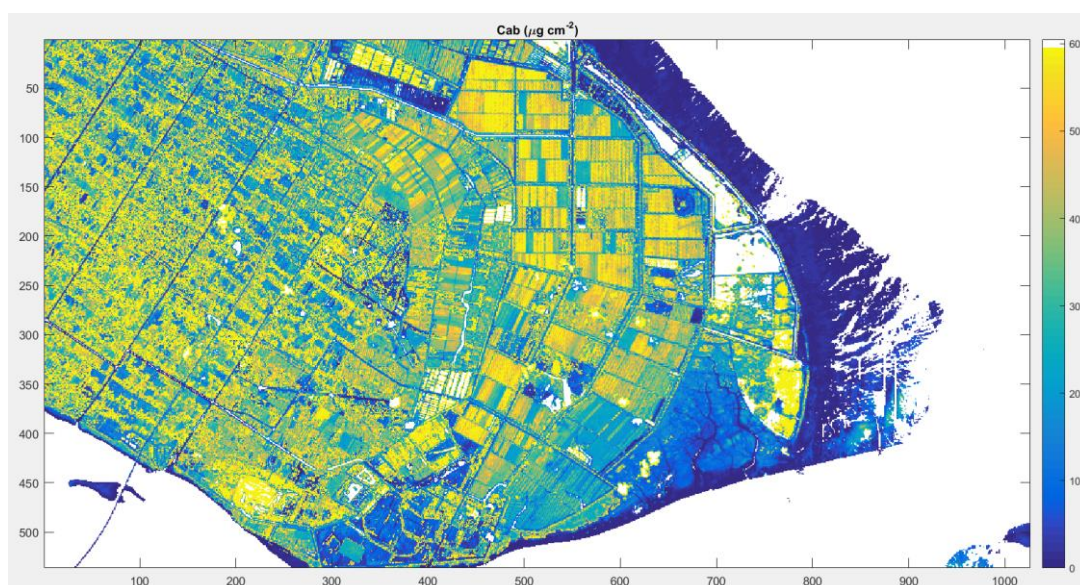
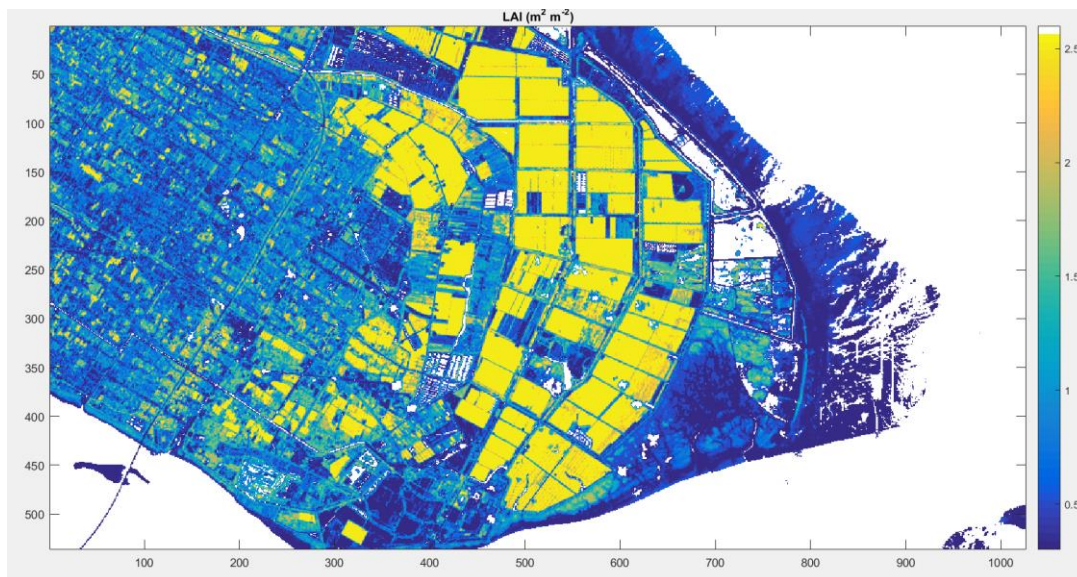


Figure 27 Map of leaf chlorophyll content ( $\mu\text{g cm}^{-2}$ ) in Chongming Dongtan

As we can see from **Figure 28**, leaf area index in coastal tidal wetland in image is no more than 2.0  $\text{m}^2 \text{m}^{-2}$  and those who have higher constant LAI values (more than 2.5  $\text{m}^2 \text{m}^{-2}$ ) resemble to agriculture farms and parks in image. Meanwhile, LAI value in urban area is almost between 1.0  $\text{m}^2 \text{m}^{-2}$  and 2.5  $\text{m}^2 \text{m}^{-2}$ . That's may be because the city green belt is well constructed.



**Figure 28** Map of LAI ( $\text{m}^2 \text{m}^{-2}$ ) in Chongming Dongtan

The map of productivity flows the mostly same trend as of leaf area index (LAI) as **Figure 29** depicted. In the whole area with urban structure, the productivity is almost between 3  $\mu\text{molm}^{-2}\text{s}^{-1}$  and 14  $\mu\text{molm}^{-2}\text{s}^{-1}$ . Productivity and LAI has a linear relationship. It can be confirmed from the map of productivity and LAI that the area with high LAI has a higher productivity.



**Figure 29** Map of productivity ( $\mu\text{molm}^{-2}\text{s}^{-1}$ ) in Chongming Dongtan

As we can see from **Figure 30**, latent heat flux calculated by SCOPE simulation and translated to Landsat 8 image illustrates higher values in vegetated areas and lower values in urban areas. In the whole map, the latent heat flux is between  $120\text{W m}^{-2}$  and  $190\text{W m}^{-2}$ . The map of latent heat flux flows the mostly same trend as of productivity especially in coastal tidal area.

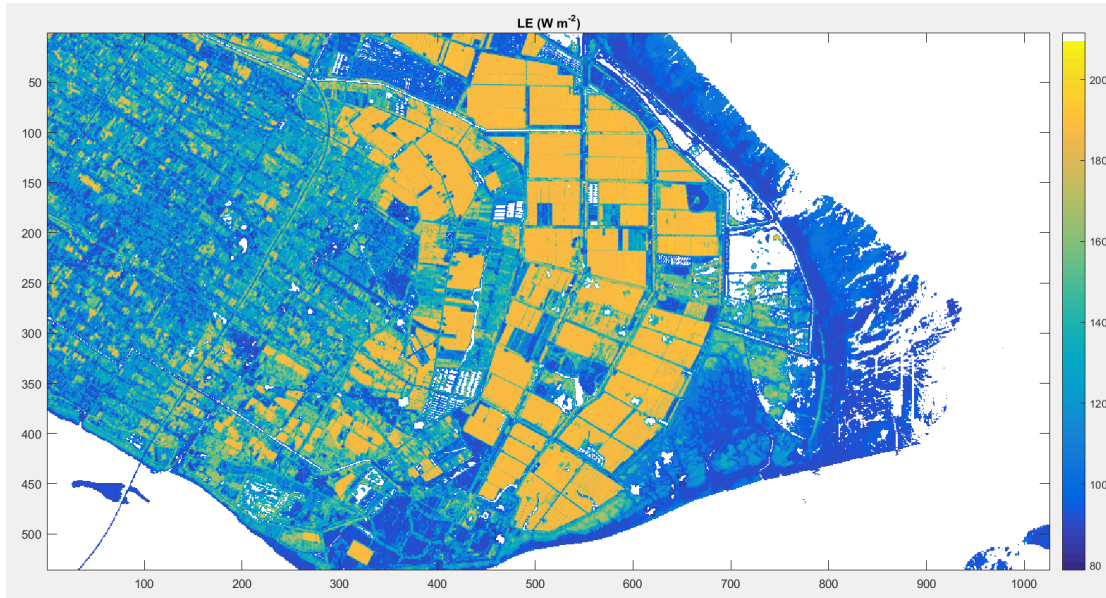


**Figure 30** Map of latent heat flux ( $\text{W m}^{-2}$ ) in Chongming Dongtan

As we can see from **Figure 31**, in the whole map, the sensible heat flux is between  $110\text{W m}^{-2}$  and  $170\text{W m}^{-2}$  while sensible heat flux is almost between  $140\text{W m}^{-2}$  and  $170\text{W m}^{-2}$  in coastal tidal wetland part. Meanwhile, the sensible heat flux of vegetated areas in coastal tidal wetland is lower than that of mudflats.



**Figure 31** Map of sensible heat flux ( $\text{W m}^{-2}$ ) in Chongming Dongtan

### 3.4. Results of Model Validation with Simulations and Measurements

#### 3.4.1. Results of Simulations with Landsat 5 TM images

Based on the **chapter 2.3.3**, the similar method could be used to obtain simulations of Landsat 5 TM images from 2005 to 2007. The purpose of deriving simulations of Landsat 5 TM images is to select the LAI and chlorophyll content values around the two flux towers. The values of LAI and chlorophyll content around the two flux towers from 2005 to 2007 are illustrated in **Table 10**.

**Table 10** The values of LAI and chlorophyll content around the two flux towers from 2005 to 2007

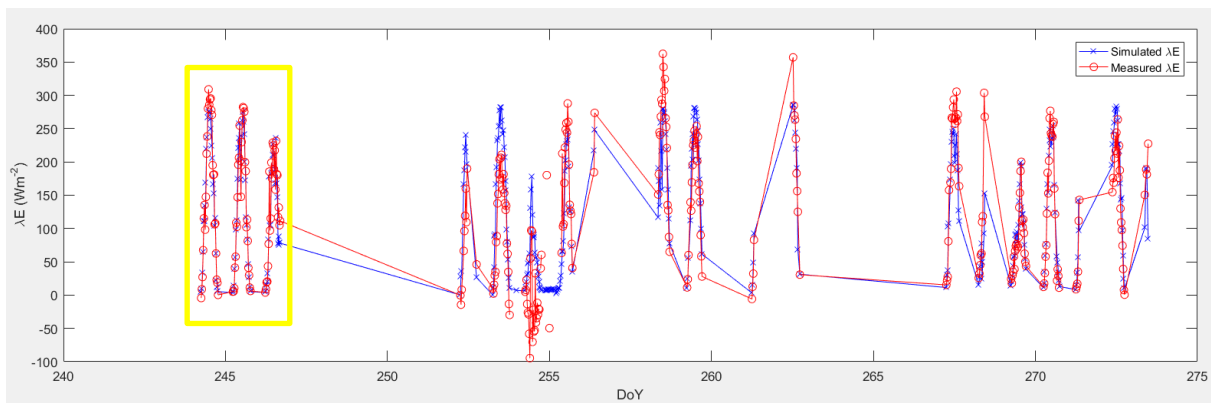
| Year                 | 2005      |           | 2006      |           | 2007      |           |
|----------------------|-----------|-----------|-----------|-----------|-----------|-----------|
| Flux tower           | Dongtan 2 | Dongtan 3 | Dongtan 2 | Dongtan 3 | Dongtan 2 | Dongtan 3 |
| Cab                  | 24.4      | 44        | 4.8       | 2         | 2         | 1.6       |
| Cca                  | 6.1       | 11        | 1.2       | 0.5       | 0.5       | 0.4       |
| LAI                  | 2.2       | 2.2       | 2.2       | 2.52      | 2.2       | 2.28      |
| Soil spectrum number | 2         | 2         | 2         | 2         | 2         | 2         |

\* Soil spectrum number refers to a retrieved soil spectrum from the five that were provided in the LUT.

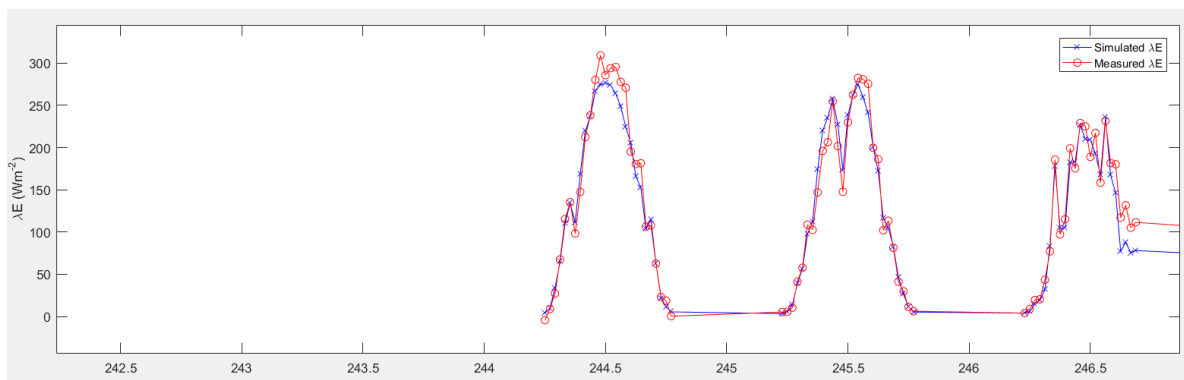
From **Table 10**, the values of those parameters could be used to carry out the time series module of SCOPE model as input data.

#### 3.4.2. Comparison of Simulation and Flux Tower Data

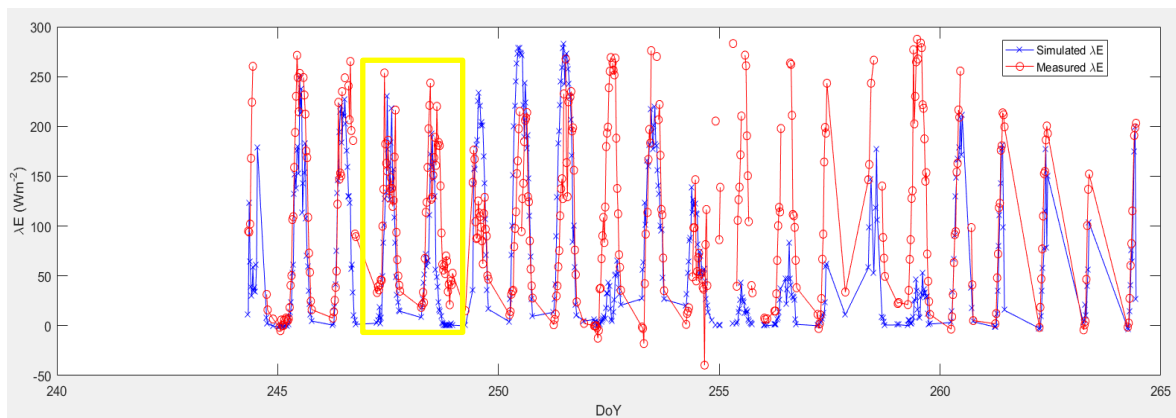
Based on the above section, fluxes were simulated for the whole September of the three years. Thus SCOPE model was executed for 6 times, assuming that the retrieved Cab and LAI could be considered representative for a month. And then the simulated time series of latent heat flux and sensible heat flux in September from 2005 to 2007 were obtained. The simulated and measured curves of latent heat flux and sensible heat flux in the two flux towers in the year of 2005 were described in **Figure 32 & Figure 33** (the curves in 2006 and 2007 were similar). The records of flux tower measurements during rainy days were removed, because during those days, the flux tower does not provide reliable data. From the two figures of the two flux towers, we can see the simulated curves of latent heat flux and sensible heat flux relatively matched measured curves of the counterparts.



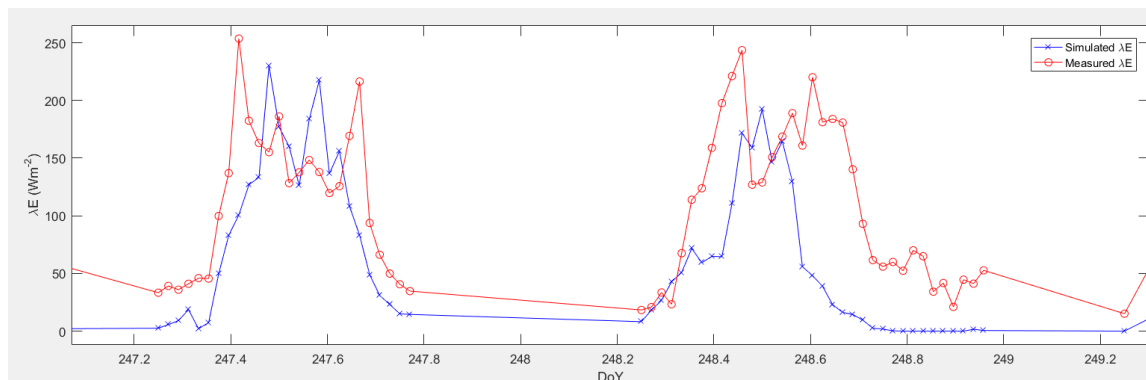
(a)



(b)

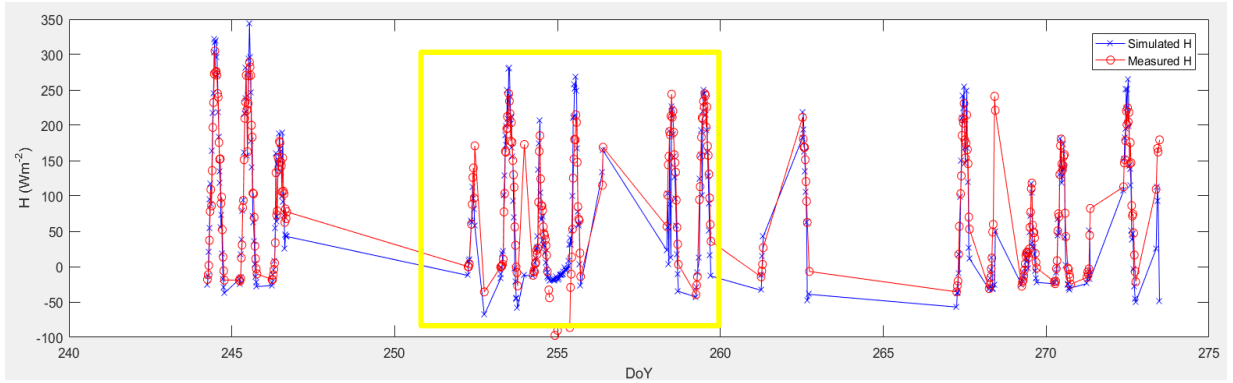


(c)

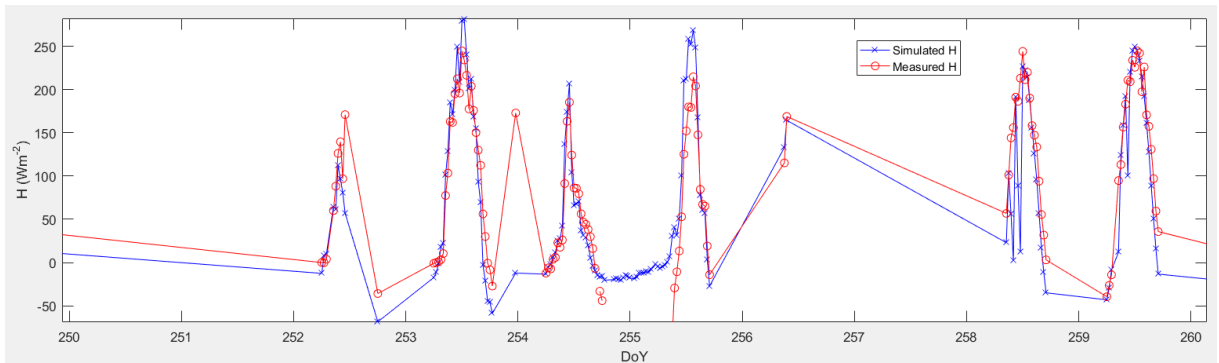


(d)

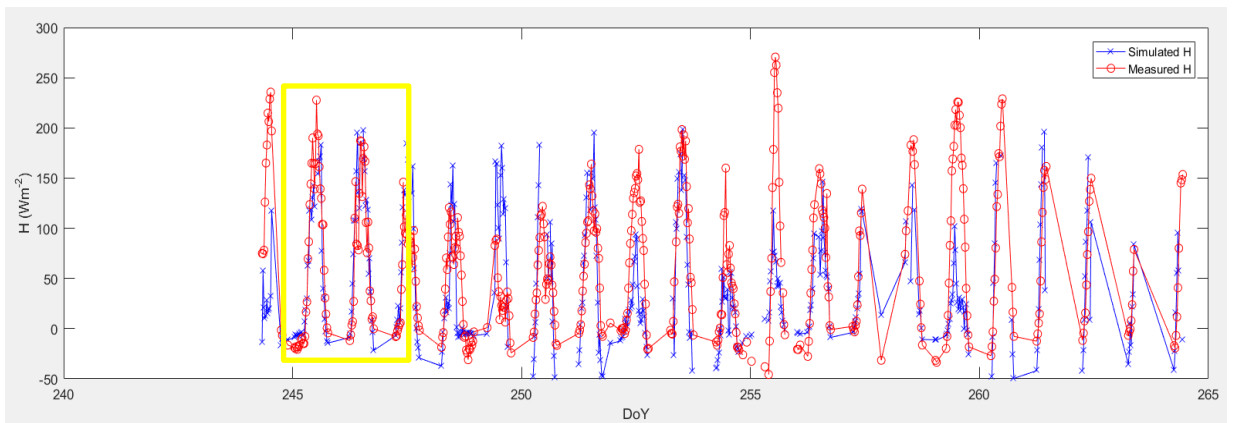
**Figure 32** The simulated and measured curves of latent heat flux in the year of 2005:  
**(a)** Dongtan 2; **(b)** Larger version of the yellow rectangle in (a); **(c)** Dongtan 3; **(d)** Larger version of the yellow rectangle in (c)



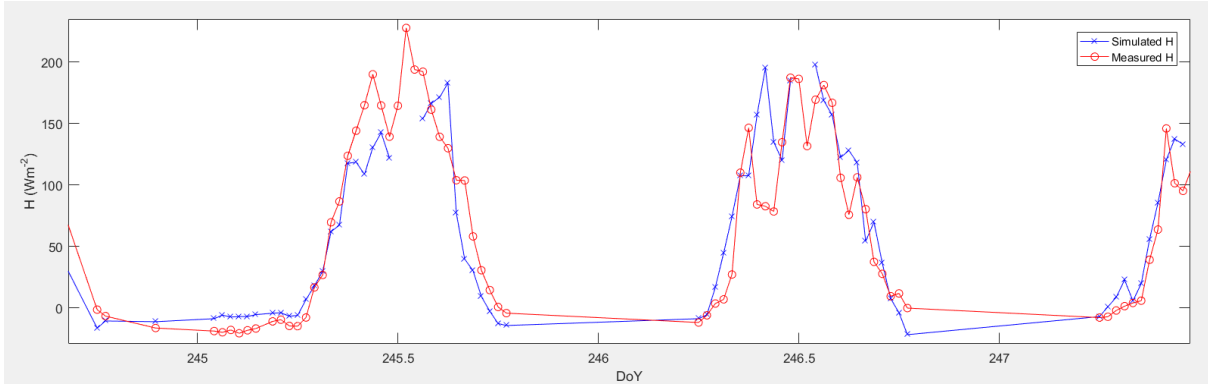
**(a)**



**(b)**



**(c)**



(d)

Figure 33 The simulated and measured curves of sensible heat flux in the year of 2005:

- (a) Dongtan 2; (b) Larger version of the yellow rectangle in (a); (c) Dongtan 3; (d) Larger version of the yellow rectangle in (c)

The RMSE values of simulated and measured of latent heat flux and sensible heat flux in the two flux towers from 2005 to 2007 are shown in **Table 11**. From following table, the RMSE values of those were all less than 65, which is satisfactory. In other words, the simulated maps of latent heat flux, sensible heat flux and vegetation parameters (LAI & Cab) can be accepted.

**Table 11** The RMSE values of simulated and measured of latent heat flux (LE) and sensible heat flux (H) in the two flux towers from 2005 to 2007

| Year       | 2005      |           | 2006      |           | 2007      |           |
|------------|-----------|-----------|-----------|-----------|-----------|-----------|
| Flux tower | Dongtan 2 | Dongtan 3 | Dongtan 2 | Dongtan 3 | Dongtan 2 | Dongtan 3 |
| RMSE of LE | 41.6768   | 64.2644   | 59.4893   | 57.0338   | 58.9731   | 55.6329   |
| RMSE of H  | 43.7321   | 58.2278   | 53.7953   | 56.5011   | 56.1336   | 54.8941   |

## 4. DISCUSSION

### 4.1. Analysis of Selecting Variable Value Range of Input Parameters in SCOPE Model Simulation

Selection of input data (Cab, Cca, LAI, soil spectra number etc.) range in SCOPE model influences the final simulations of mapping profoundly. Therefore, three different combinations of input data of SCOPE model are discussed as follows as alternatives for building the LUT:

#### ➤ Combination of 46 measuring points

Based on **Chapter 3.2**, the simulated 4 soil parameters (B, lat, lon and Smp) and 9 vegetation parameters (Cab, Cca, Cmd, Cw, Cs, N, LIDFa, LIDFb, LAI) of 46 measuring points from RTMo have been obtained. The simulated maps of productivity, latent heat flux, sensible heat flux, LAI and chlorophyll can be obtained as **Figure 34** illustrates through individual run of SCOPE model with all the parameters of 46 measuring points as input data in the LUT.

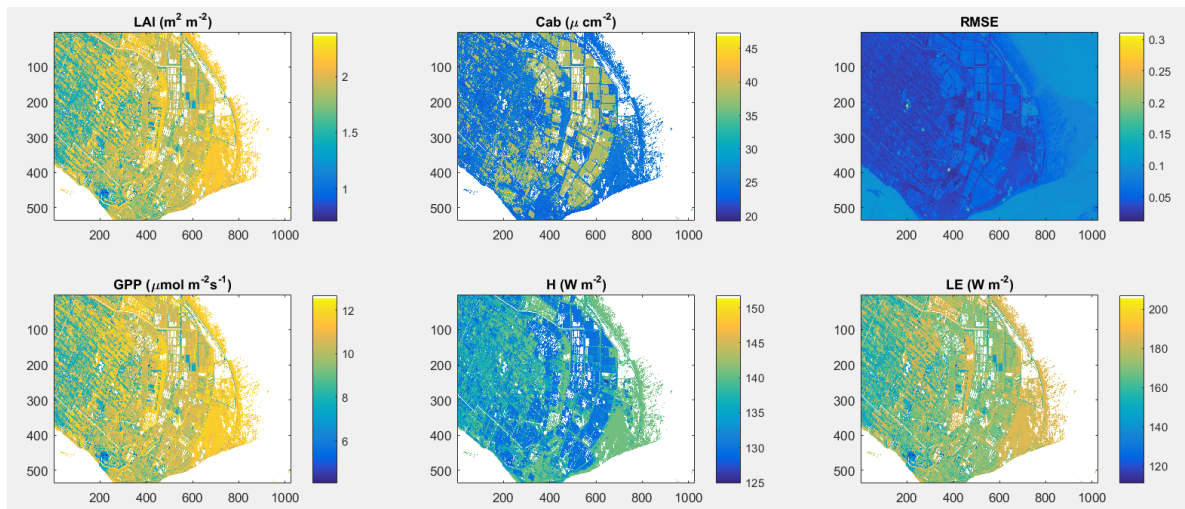


**Figure 34** The simulated maps of productivity, latent heat flux, sensible heat flux, LAI, chlorophyll and RMSE with combination of 46 measuring points

As **Figure 34** depicts, although RMSE value is no more than 0.05 along coastal tidal wetland, the values of productivity, latent heat flux, sensible heat flux, LAI and chlorophyll in coastal tidal wetland are not changed so much. However, actually mudflats account for a large part of wetland in September. Therefore, the values of LAI and chlorophyll should not be high and similar along coastal tidal wetland. An LUT of only 46 combinations cannot represent the whole area well.

➤ **Combination of LAI & chlorophyll without 0 value**

Based on **chapter 3.2**, the maximum and minimum of LAI and chlorophyll of three vegetation types have been obtained. In this scenario, the maximum as the upper bound, and the minimum as the lower bound were selected (SCOPE model cannot run with LAI=0, while RTMo can run with LAI=0). The values of Cab and LAI are described in **Table 12**. The simulated maps of productivity, latent heat flux, sensible heat flux, LAI and chlorophyll can be obtained as **Figure 35**.

**Table 12** The values selection of Cab and LAI in SCOPE model input data

| Parameter | Value Selection |      |      |     |      | Count |
|-----------|-----------------|------|------|-----|------|-------|
| Cab       | 15              | 16   | 17   | ... | 60   | 46    |
| LAI       | 0.34            | 0.44 | 0.54 | ... | 2.54 | 23    |

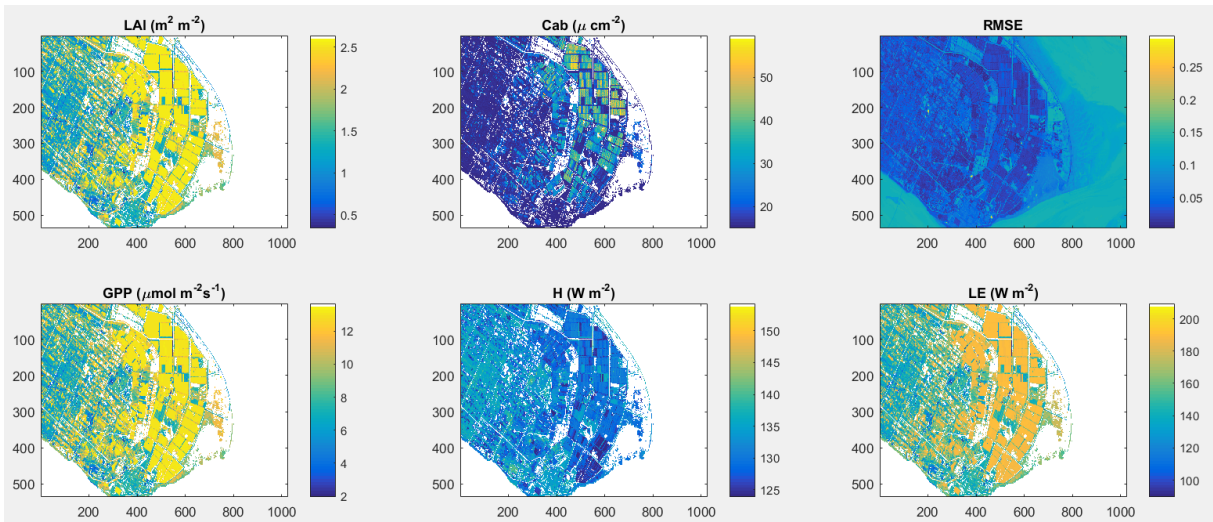


**Figure 35** The simulated maps of productivity, latent heat flux, sensible heat flux, LAI, chlorophyll and RMSE with combination of LAI & chlorophyll without 0 value

As **Figure 35** shows, the simulated maps are better than those of the combination of 46 measuring points. However, the mudflats were also not simulated satisfyingly. The cause is that the simulation has not contained mudflats' properties and SCOPE cannot simulate well in such conditions.

➤ **Combination of Soil spectrums, LAI & chlorophyll with 0 value**

Based on the above two combinations, the input data as **Table 9** has been selected. The simulated maps of productivity, latent heat flux, sensible heat flux, LAI and chlorophyll can be obtained as **Figure 26-31**.

#### 4.2. Explanation of Abnormal Reflectance Spectrums in SCOPE Model Simulation

For the SCOPE model simulation, the Look-up table option to run SCOPE was adopted. The simulated reflectance spectra were shown in **Figure 23**, and some of the spectra at the wavelength between 400nm and 900 nm are quite abnormal (**Figure 36**). The causes of those abnormal spectra are a couple of possibilities of unrealistic parameter combinations: (1) Carotenoid content (Cca) which is usually 25% of Cab might be higher than Cab in simulations; (2) The values of Cab and Cca are not 0 in mudflat parts, etc. However, when searching for the minimum in Equation 2, these abnormal spectra will not be selected.

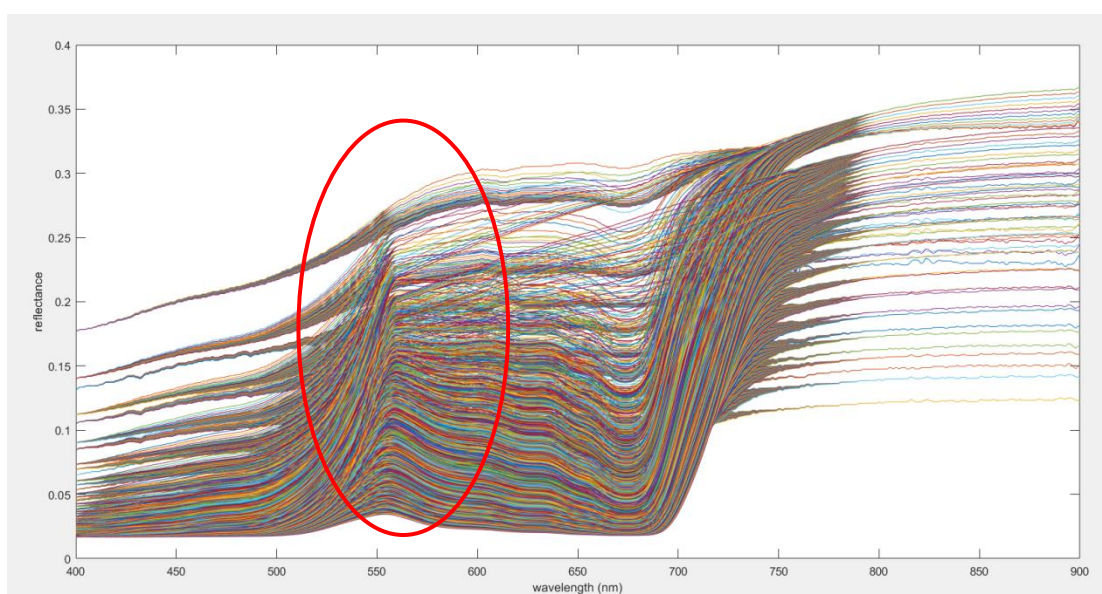


**Figure 36** The simulated reflectance spectrums at the wavelength between 400nm and 900 nm

#### 4.3. Reasons for the Uncertainties of Mapping with SCOPE Model

Based on the **chapter 3.3.3**, there was masked part in simulated maps of productivity, latent heat flux, sensible heat flux, LAI and chlorophyll for which RMSE of the simulated Landsat 8 OLI reflectance exceeded 0.05. As for the reasons for removing the parts of which RMSE value is more than 0.05 can be found in comparing Landsat 8 OLI image (**Figure 17**) in natural color composite with the simulated maps before removing (**Figure 37**). From **Figure 37**, actually LAI value in the mudflats and ocean parts should be 0, but they had nonzero value in the simulated LAI map. Therefore, the incorrect part should be removed. When RMSE value is more than 0.05, the clouds, unrealistic mudflat and ocean parts can be all masked. Therefore, a limit of RMSE of 0.05 was used.

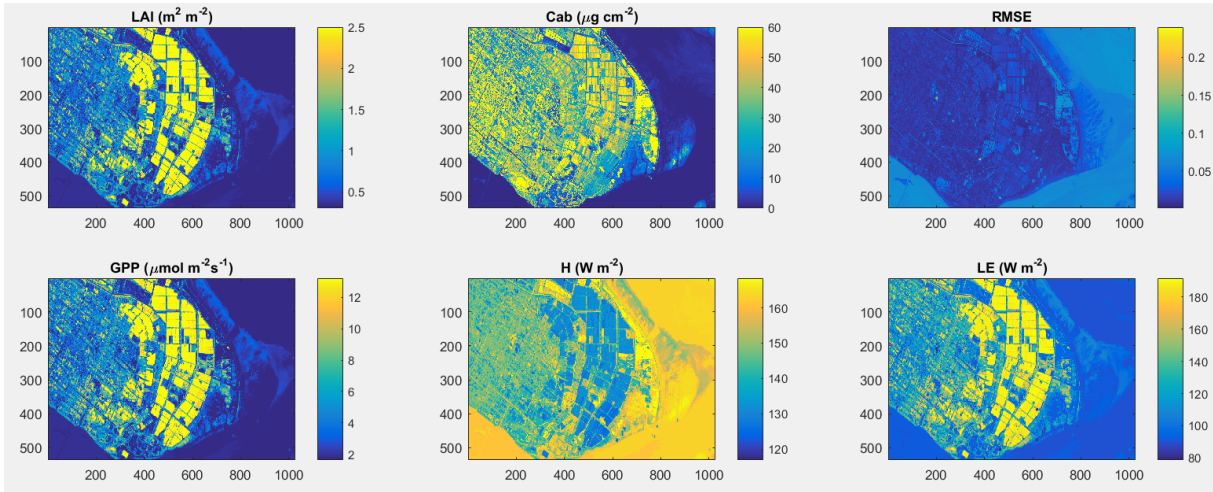


Figure 37 The simulated maps of productivity, latent heat flux, sensible heat flux, LAI, chlorophyll and RMSE before removing

To be more specific, we can select two points (one is in vegetated area ( $RMSE < 0.02$ ), and the other is in mudflats ( $RMSE > 0.1$ )) in the simulated map to analyse the simulated accuracy of different areas. The two points the author selected were depicted in **Figure 38**.

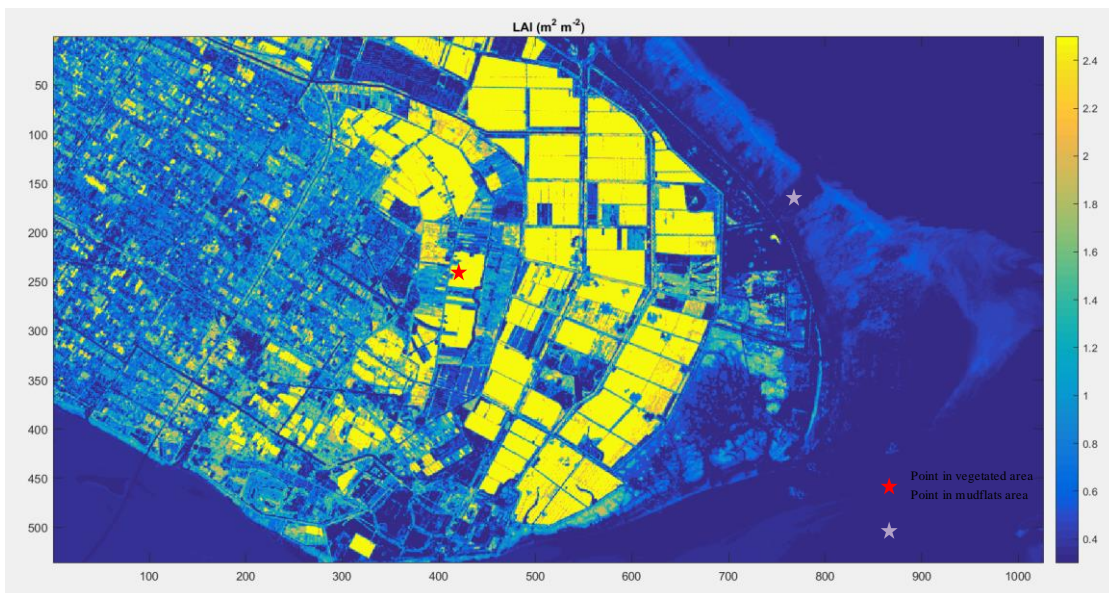


Figure 38 The simulated maps of LAI with two selecting points

➤ **Point in vegetated area**

I selected (411,265) in the map as a point in vegetated area of which RMSE value equals to 0.00998 and LAI value equals to 2.36. **Figure 39** illustrates the 5 simulated reflectance spectrums and pixel values in 7 bands of Landsat 8 of that point in vegetated area.

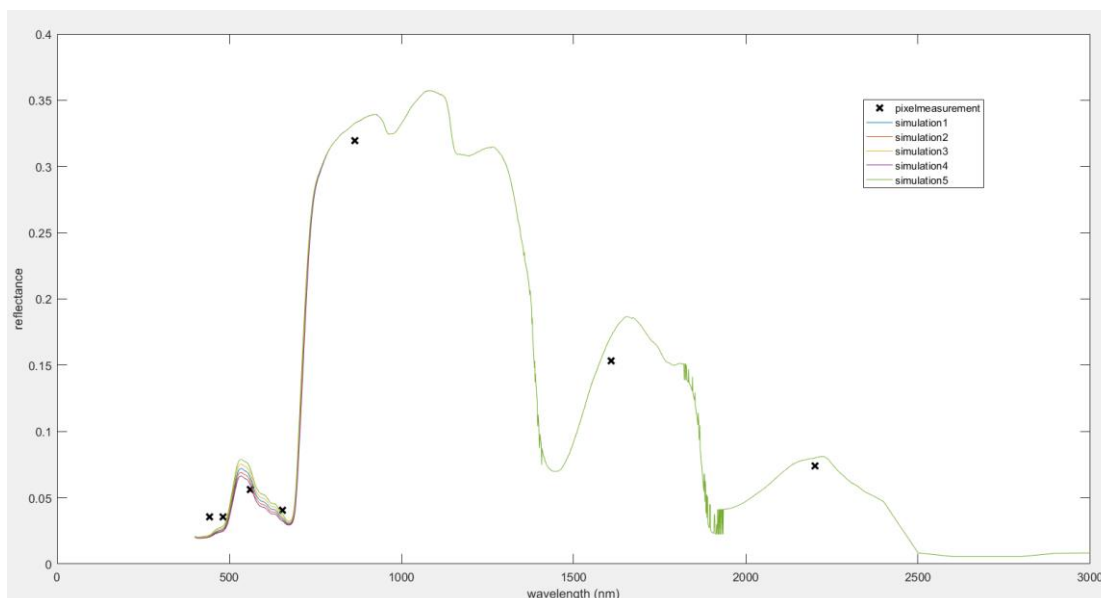


Figure 39 The 5 simulated reflectance spectrums and pixel values in 7 bands of Landsat 8 in vegetated area

#### ➤ Point in mudflats area

I selected (762,171) in the map as a point in vegetated area of which RMSE value equals to 0.1212 and LAI value equals to 2.2. **Figure 40** illustrates the 5 simulated reflectance spectrums and pixel values in 7 bands of Landsat 8 of that point in mudflats area.

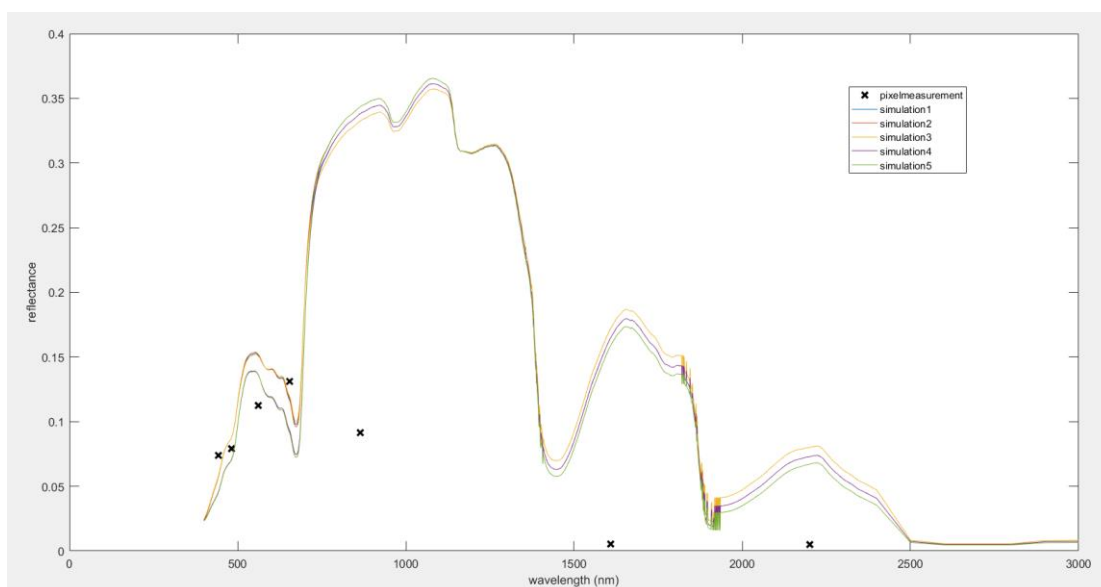


Figure 40 The 5 simulated reflectance spectrums and pixel values in 7 bands of Landsat 8 in mudflats area

In brief, through comparing the above specific simulations of two points, the reasons for the uncertainties of SCOPE model simulations can be found as follow: (1) meteorological influence; (2)

insufficiency of input data of soil properties; (3) the quality and quantity of field work data; (4) the number of simulated combinations. If the above problems can be improved, the simulated results could improve.

## 5. CONCLUSION

Initially, in the case of the differences of in situ measured spectral signatures of the different vegetation types and the mudflats, the peak value of *Spartina alterniflora* reflectance spectrum is the highest, whereas *Phragmites australis* is the second, *Scirpus mariqueter* is the third and the mudflat is the lowest one. Meanwhile, the reflectance values of *Scirpus mariqueter* and *Phragmites australis* spectrums are lower than those commonly found for vegetated areas. This may be caused by the dark soil background and low leaf area index.

Moreover, the causes of the differences between Landsat 8 TOC reflectance and in situ reflectance in the same pixel are: (1) meteorological influence (atmospheric influence of Landsat 8 image and weather influence in field work data collection); (2) spatial resolution; (3) the quantity of field work data.

Furthermore, in terms of LAI and chlorophyll value, mudflats should be 0, whereas the counterparts of vegetation are around  $1 \text{ m}^2 \text{ m}^{-2} - 2 \text{ m}^2 \text{ m}^{-2}$  and  $5 \mu\text{g cm}^{-2} - 60 \mu\text{g cm}^{-2}$  respectively. As for the values of latent heat flux and productivity, mudflats are lower than vegetation. However, the values of sensible heat flux of mudflats are higher than that of vegetation.

Last but not least, the uncertainties of the productivity (photosynthesis) product of the SCOPE model from Landsat 8 are: (1) uncertain meteorological condition (only an example of meteorological condition in SCOPE input data, not the real weather for study area); (2) insufficient simulation of mudflats; (3) the quality and quantity of field work data; (4) the number of simulated combinations.

For further study, if the quality and quantity of field work data can be improved, and soil properties and meteorological condition can be obtained, the results of mapping protocol of biophysical and biochemical properties in Chongming Dongtan wetland for environmental protection and restoration as well as assessment and monitoring will be much better.



## LIST OF REFERENCES

---

- Bhuiyan, M. J. A. N., & Dutta, D. (2012). Analysis of flood vulnerability and assessment of the impacts in coastal zones of Bangladesh due to potential sea-level rise. *Natural Hazards*, 61(2), 729–743.  
<http://doi.org/10.1007/s11069-011-0059-3>
- Chen, J., Wang, L., Li, Y., Zhang, W., Fu, X., & Le, Y. (2012). Effect of *Spartina alterniflora* invasion and its controlling technologies on soil microbial respiration of a tidal wetland in Chongming Dongtan, China. *Ecological Engineering*, 41, 52–59. <http://doi.org/10.1016/j.ecoleng.2012.01.024>
- Chonglin, X. (2009). Mapping wetland vegetation and estimating its biophysical characteristics using C - band ENVISAT ASAR in Poyang Lake, China, (March).
- de Almeida, T. I. R., Penatti, N. C., Ferreira, L. G., Arantes, A. E., & do Amaral, C. H. (2015). Principal component analysis applied to a time series of MODIS images: the spatio-temporal variability of the Pantanal wetland, Brazil. *Wetlands Ecology and Management*, 23(4), 737–748.  
<http://doi.org/10.1007/s11273-015-9416-4>
- Dronova, I., Gong, P., & Wang, L. (2011). Object-based analysis and change detection of major wetland cover types and their classification uncertainty during the low water period at Poyang Lake, China. *Remote Sensing of Environment*, 115(12), 3220–3236. <http://doi.org/10.1016/j.rse.2011.07.006>
- Duffour, C., Olioso, A., Demarty, J., Van der Tol, C., & Lagouarde, J. P. (2015). An evaluation of SCOPE: A tool to simulate the directional anisotropy of satellite-measured surface temperatures. *Remote Sensing of Environment*, 158, 362–375. <http://doi.org/10.1016/j.rse.2014.10.019>
- Ghosh, S., Mishra, D. R., & Gitelson, A. A. (2016). Long-term monitoring of biophysical characteristics of tidal wetlands in the northern Gulf of Mexico - A methodological approach using MODIS. *Remote Sensing of Environment*, 173, 39–58. <http://doi.org/10.1016/j.rse.2015.11.015>
- Gilmore, M. S., Wilson, E. H., Barrett, N., Civco, D. L., Prisløe, S., Hurd, J. D., & Chadwick, C. (2008). Integrating multi-temporal spectral and structural information to map wetland vegetation in a lower Connecticut River tidal marsh. *Remote Sensing of Environment*, 112(11), 4048–4060.  
<http://doi.org/10.1016/j.rse.2008.05.020>
- Goudie, A. (2013). Characterising the distribution and morphology of creeks and pans on salt marshes in England and Wales using Google Earth. *Estuarine, Coastal and Shelf Science*, 129, 112–123.  
<http://doi.org/10.1016/j.ecss.2013.05.015>
- Guo, C., & Guo, X. (2016). Estimating leaf chlorophyll and nitrogen content of wetland emergent plants using hyperspectral data in the visible domain. *Spectroscopy Letters*, 49(3), 180–187.  
<http://doi.org/10.1080/00387010.2015.1118126>
- Heumann, B. W., Hackett, R. A., & Monfils, A. K. (2015). Testing the spectral diversity hypothesis using spectroscopy data in a simulated wetland community. *Ecological Informatics*, 25, 29–34.  
<http://doi.org/10.1016/j.ecoinf.2014.10.005>

- Hong, S. H., Kim, H. O., Wdowinski, S., & Feliciano, E. (2015). Evaluation of polarimetric SAR decomposition for classifying wetland vegetation types. *Remote Sensing*, 7(7), 8563–8585. <http://doi.org/10.3390/rs70708563>
- Hu, Y., Wang, L., Fu, X., Yan, J., Wu, J., Tsang, Y., ... Sun, Y. (2016). Salinity and nutrient contents of tidal water affects soil respiration and carbon sequestration of high and low tidal flats of Jiuduansha wetlands in different ways. *Science of The Total Environment*, 565, 637–648. <http://doi.org/10.1016/j.scitotenv.2016.05.004>
- Jacquemoud, S., Verhoef, W., Baret, F., Bacour, C., Zarco-tejada, P. J., Asner, G. P., ... Ustin, S. L. (2009). Remote Sensing of Environment PROSPECT + SAIL models : A review of use for vegetation characterization. *Remote Sensing of Environment*, 113, S56–S66. <http://doi.org/10.1016/j.rse.2008.01.026>
- Kearney, M. S., Stutzer, D., Turpie, K., & Stevenson, J. C. (2009). The Effects of Tidal Inundation on the Reflectance Characteristics of Coastal Marsh Vegetation. *Journal of Coastal Research*, 25(256), 1177–1186. <http://doi.org/10.2112/08-1080.1>
- Levin, N., Elron, E., & Gasith, A. (2009). Decline of wetland ecosystems in the coastal plain of Israel during the 20th century: Implications for wetland conservation and management. *Landscape and Urban Planning*, 92(3-4), 220–232. <http://doi.org/10.1016/j.landurbplan.2009.05.009>
- Li, X., Zhou, Y., Zhang, L., & Kuang, R. (2014). Shoreline change of Chongming Dongtan and response to river sediment load: A remote sensing assessment. *Journal of Hydrology*, 511, 432–442. <http://doi.org/10.1016/j.jhydrol.2014.02.013>
- Lin, W., & Chen, N. (2009). Inversion of leaf area index for invasive plant using ENVISAT ASAR. *Urban Remote Sensing Joint Event*.
- M.J.A. Butler, M.-C. Mouchot, V. Barale, C. L. (1988). *The application of remote sensing technology to marine fisheries: an introductory manual*. FOOD AND AGRICULTURE ORGANIZATION OF THE UNITED NATIONS Rome.
- Mishra, D. R., Cho, H. J., Ghosh, S., Fox, A., Downs, C., Merani, P. B. T., ... Mishra, S. (2012). Post-spill state of the marsh: Remote estimation of the ecological impact of the Gulf of Mexico oil spill on Louisiana Salt Marshes. *Remote Sensing of Environment*, 118, 176–185. <http://doi.org/10.1016/j.rse.2011.11.007>
- Mishra, D. R., Ghosh, S., Hladik, C., O'Connell, J., & Cho, H. J. (2015). Wetland Mapping Methods and Techniques Using Multisensor, Multiresolution Remote Sensing: Successes and Challenges. *Remote Sensing of Water Resources, Disasters, and Urban Studies*, (JANUARY 2015), 191–226. <http://doi.org/doi:10.1201/b19321-13>
- Mutanga, O., Adam, E., & Cho, M. A. (2012). High density biomass estimation for wetland vegetation using worldview-2 imagery and random forest regression algorithm. *International Journal of Applied Earth Observation and Geoinformation*, 18(1), 399–406. <http://doi.org/10.1016/j.jag.2012.03.012>

- Pengra, B. W., Johnston, C. A., & Loveland, T. R. (2007). Mapping an invasive plant, *Phragmites australis*, in coastal wetlands using the EO-1 Hyperion hyperspectral sensor. *Remote Sensing of Environment*, *108*(1), 74–81. <http://doi.org/10.1016/j.rse.2006.11.002>
- Prosperre, K., McLaren, K., & Wilson, B. (2014). Plant species discrimination in a tropical wetland using in situ hyperspectral data. *Remote Sensing*, *6*(9), 8494–8523. <http://doi.org/10.3390/rs6098494>
- RAHMAN & DEDIEU. (1994). SMAC - A SIMPLIFIED METHOD FOR THE ATMOSPHERIC CORRECTION OF SATELLITE MEASUREMENTS IN THE SOLAR SPECTRUM. *INTERNATIONAL JOURNAL OF REMOTE SENSING*, *15*(1), 123–143.
- Siciliano, D., Wasson, K., Potts, D. C., & Olsen, R. C. (2008). Evaluating hyperspectral imaging of wetland vegetation as a tool for detecting estuarine nutrient enrichment. *Remote Sensing of Environment*. Retrieved from C:\gwhite\Hg Biblio\attachments\Evaluating hyperspectral imaging of wetland vegetation as a tool for detecting estuarine nutrient enrichment.pdf
- Sieben, E. J. J., Collins, N. B., Mtshali, H., & Venter, C. E. (2016). The vegetation of inland wetlands with salt-tolerant vegetation in South Africa: Description, classification and explanatory environmental factors. *South African Journal of Botany*, *104*, 199–207. <http://doi.org/10.1016/j.sajb.2015.11.004>
- Tana, G., Letu, H., Cheng, Z., & Tateishi, R. (2013). Wetlands mapping in north america by decision rule classification using MODIS and ancillary data. *IEEE Journal of Selected Topics in Applied Earth Observations and Remote Sensing*, *6*(6), 2391–2401. <http://doi.org/10.1109/JSTARS.2013.2249499>
- Tian, J. H., Wang, J. H., Liu, Z. C., Li, H. C., Wang, X. Z., Xie, D. Y., ... Yu, X. J. (2010). A conceptual ecological model of Cangzhou coastal wetlands, Hebei Province, China. *Procedia Environmental Sciences*, *2*, 1002–1011. <http://doi.org/10.1016/j.proenv.2010.10.112>
- Timmermans, J., Su, Z., Van Der Tol, C., Verhoef, A., & Verhoef, W. (2013). Quantifying the uncertainty in estimates of surface-atmosphere fluxes through joint evaluation of the SEBS and SCOPE models. *Hydrology and Earth System Sciences*, *17*(4), 1561–1573. <http://doi.org/10.5194/hess-17-1561-2013>
- Tol, C. Van Der, Rossini, M., Cogliati, S., Verhoef, W., & Colombo, R. (2016). Remote Sensing of Environment A model and measurement comparison of diurnal cycles of sun-induced chlorophyll fluorescence of crops. *Remote Sensing of Environment*, *186*, 663–677. <http://doi.org/10.1016/j.rse.2016.09.021>
- Turpie, K. R., Klemas, V. V., Byrd, K., Kelly, M., & Jo, Y. H. (2015). Prospective HypsIRI global observations of tidal wetlands. *Remote Sensing of Environment*, *167*, 206–217. <http://doi.org/10.1016/j.rse.2015.05.008>
- Tuxen, K., Schile, L., Stralberg, D., Siegel, S., Parker, T., Vasey, M., ... Kelly, M. (2011). Mapping changes in tidal wetland vegetation composition and pattern across a salinity gradient using high spatial resolution imagery. *Wetlands Ecology and Management*. <http://doi.org/10.1007/s11273-010-9207-x>
- van der Tol, C., Verhoef, W., Timmermans, J., Verhoef, a., & Su, Z. (2009). An integrated model of soil-canopy spectral radiances, photosynthesis, fluorescence, temperature and energy balance. *Biogeosciences*, *6*(12), 3109–3129. <http://doi.org/10.5194/bg-6-3109-2009>

- Wentao, Z., Bingfang, W., Hongbo, J., & Hua, L. (2014). Texture classification of vegetation cover in high altitude wetlands zone. *Conf. Series: Earth and Environmental Science*, 17, 012083.  
<http://doi.org/10.1088/1755-1315/17/1/012083>
- Wigand, C., Carlisle, B., Smith, J., Carullo, M., Fillis, D., Charpentier, M., ... Heltshe, J. (2011). Development and validation of rapid assessment indices of condition for coastal tidal wetlands in southern New England, USA. *Environmental Monitoring and Assessment*, 182(1-4), 31–46.  
<http://doi.org/10.1007/s10661-010-1856-y>
- Wright, C., & Gallant, A. (2007). Improved wetland remote sensing in Yellowstone National Park using classification trees to combine TM imagery and ancillary environmental data. *Remote Sensing of Environment*, 107(4), 582–605. <http://doi.org/10.1016/j.rse.2006.10.019>
- Zhang, S., Wang, L., Hu, J., Zhang, W., Fu, X., Le, Y., & Jin, F. (2011). Organic carbon accumulation capability of two typical tidal wetland soils in Chongming Dongtan, China. *Journal of Environmental Sciences*, 23(1), 87–94. [http://doi.org/10.1016/S1001-0742\(10\)60377-4](http://doi.org/10.1016/S1001-0742(10)60377-4)
- Zheng, Z., Zhou, Y., Tian, B., & Ding, X. (2016). The spatial relationship between salt marsh vegetation patterns, soil elevation and tidal channels using remote sensing at Chongming Dongtan Nature Reserve, China. *Acta Oceanologica Sinica*, 35(4), 26–34. <http://doi.org/10.1007/s13131-016-0831-z>
- Zhong, Q., Wang, K., Lai, Q., Zhang, C., & Zheng, L. (2016). Carbon Dioxide Fluxes and Their Environmental Control in a Reclaimed Coastal Wetland in the Yangtze Estuary, 344–362.  
<http://doi.org/10.1007/s12237-015-9997-4>
- Zou, Y. A., Tang, C. D., Niu, J. Y., Wang, T. H., Xie, Y. H., & Guo, H. (2016). Migratory Waterbirds Response to Coastal Habitat Changes: Conservation Implications from Long-term Detection in the Chongming Dongtan Wetlands, China. *Estuaries and Coasts*, 39(1), 273–286.  
<http://doi.org/10.1007/s12237-015-9991-x>